NASA CR 72728

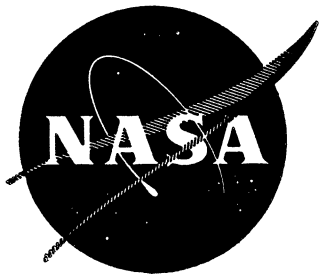


# STUDIES OF DYNAMIC CONTACT ANGLES ON SOLIDS

by

Anthony M. Schwartz and Silvestre B. Tejada

THE GILLETTE COMPANY RESEARCH INSTITUTE
1413 Research Boulevard
Rockville, Maryland 20850

prepared for

## National Aeronautics and Space Administration

CONTRACT NAS3-11522

NASA Lewis Research Center
Cleveland, Ohio
Donald A. Petrash, Project Manager
Spacecraft Technology Division

NOTICE

This report was prepared as an account of Government sponsored work. Neither the United States, nor the National Aeronautics and Space Administration (NASA), nor any person acting on behalf of NASA:

A.) Makes any warranty or representation, expressed or implied, with respect to the accuracy, completeness, or usefulness of the information contained in this report, or that the use of any information, apparatus, method, or process disclosed in this report may not infringe privately owned rights; or

B.) Assumes any liabilities with respect to the use of, or for damages resulting from the use of, any information, apparatus, method or process disclosed in this report.

As used above, "person acting on behalf of NASA" includes any employee or contractor of NASA, or employee of such contractor, to the extent that such employee or contractor of NASA, or employee of such contractor prepares, disseminates, or provides access to, any information pursuant to his employment or contract with NASA, or his employment with such contractor.

Requests for copies of this report should be referred to

National Aeronautics and Space Administration
Scientific and Technical Information Facility
P. O. Box 33
College Park, MD. 20740

NASA CR 72728

Final Report

# STUDIES OF DYNAMIC CONTACT ANGLES ON SOLIDS

by

Anthony M. Schwartz and Silvestre B. Tejada

THE GILLETTE COMPANY RESEARCH INSTITUTE
1413 Research Boulevard
Rockville, Maryland 20850

prepared for

## National Aeronautics and Space Administration

July 7, 1970

CONTRACT NAS3-11522

NASA Lewis Research Center
Cleveland, Ohio
Donald A. Petrash, Project Manager
Spacecraft Technology Division

TABLE OF CONTENTS

## ABSTRACT

The relationship between dynamic contact angle ($\theta_d$) and velocity of the liquid front along a solid surface was studied for ten different liquid-solid combinations. Some of these combinations had an equilibrium contact angle ($\theta_{eq}$) of zero; others had $\theta_{eq}$ positive. The surface of the solid in each combination was roughened to varying degrees so that the effect of variations in roughness on the $\theta_d$-V relationship might be ascertained. Variation in $\theta_{eq}$ appeared to have no effect on the form of the $\theta_d$-V relationship. The degree of roughness had no appreciable effect, except when the process of roughening (abrasion) had presumably changed the physicochemical character of the surface. The form of the $\theta_d$-V relationship changed with the velocity. Starting from V = 0 two of the solid-liquid combinations showed a region in which $\theta_d = \theta_{eq}$. Immediately above this region these and all the other solid-liquid combinations behaved according to the theoretical equation of Blake and Haynes, which is based on the concept of liquid molecules sliding along the solid surface. The parameters in this equation are characteristic of the liquid-solid combination rather than of the liquid alone. At still higher velocities the $\theta_d$-V relationship was describable by an equation of the form proposed by Friz. This represents a surging motion of the liquid superimposed on the sliding motion. In the surging mode the governing parameters are characteristic of the liquid only.

## SUMMARY

The relationship between dynamic contact angle ($\theta_d$) and velocity (V) of the liquid-solid-vapor boundary line along the solid surface, was studied for ten different liquid-solid systems. In all ten systems the solid was used in the smooth state and at three different degrees of roughness. The roughness was produced by blasting with abrasive grit of three different sizes, and the degree of roughness of the three specimens was approximately 30, 20 and 12 microinches respectively. Five of the systems had an equilibrium contact angle ($\theta_{eq}$) of zero and the other five had equilibrium contact angles ranging from 16° to 70°. The velocity range varied somewhat from system to system but generally covered about 2.5-3 decades in the range .02-20 cm/sec. At the highest velocities used the dynamic contact angle was not greater than 90°.

It was found that the form of the $\theta_d$-V relationship was the same for systems of zero $\theta_{eq}$ as for systems of positive $\theta_{eq}$.

Degree of roughness, i.e. the small-scale geometrical form of the surface, appeared to have no significant qualitative or quantitative effect on the $\theta_d$-V relationship, provided the surfaces had been roughened by the same procedure. Starting with a smooth surface and roughening it by abrasion can change its physicochemical character as well as its geometry. This change did appear to influence the $\theta_d$-V behavior in some of the systems, but not in others.

The data were also analysed to determine the functional form of the $\theta_d$-V relationship and the nature of the governing parameters. It was found that for all but two of the systems the relationship in the low velocity region was described very well by an equation derived on theoretical grounds by Blake and Haynes (ref. 16):

$$V = 2K\lambda \sinh\left[\frac{\gamma_{LV}}{\Delta nkT}\left(\cos\theta_{eq} - \cos\theta_d\right)\right]$$

This equation, based on the theory of absolute reaction rates, describes a sliding motion of the liquid molecules along the solid surface. The key

parameters K, $\lambda$ and $\Delta n$ represent, respectively, the frequency of molecular jumps, the length of each jump, and the concentration of available sites for the molecules to land on. These are properties of the specific liquid-solid combination. $\gamma_{LV}$ is the surface tension of the liquid and $\theta_{eq}$ is the equilibrium contact angle.

Above a certain critical velocity (which is higher the lower the viscosity of the liquid) the $\theta_d$-V relationship was better described by an equation of the general form given by Friz (ref. 13):

$$\tan\theta_d = a\left(\frac{\eta}{\gamma_{LV}} \cdot V\right)^b$$

where a and b are constants (b having a value which ranges from as low as .1 to as high as .8 or more, depending on the system) and $\eta$ is the bulk viscosity of the liquid. This corresponds to a surging motion of the liquid superposed on the sliding motion characteristic of the lower velocities.

Two systems, both involving the low viscosity, low-boiling, non-polar liquid hexane, showed a considerable region starting at V = 0 in which $\theta_d$ remained equal to $\theta_{eq}$ before rising suddenly and starting to follow the behavior of the other systems. This is the type of dynamic contact angle behavior at lowest velocities described by Elliott and Riddiford (refs. 10, 11).

## INTRODUCTION

The problem of controlling the flow of liquids in and out of containers at zero gravity depends on certain aspects of capillarity that have relatively little applicability under normal terrestrial gravity, and about which little information has previously been available. One of these is the dynamic contact angle, which at zero gravity becomes an important factor in the sloshing of liquids against container walls and in damping the surface disturbances that accompany the sloshing. In previous work (ref. 1) the dynamic contact angle behavior (i.e. contact angle vs. velocity of the liquid-solid-vapor line along the solid surface) of twenty-five different liquid-solid-vapor systems was studied. These systems involved combinations of seven different liquids and five different solids. The static equilibrium contact angle of all these systems was zero, and the solid surfaces were smooth by usual engineering standards. As part of that study an empirical equation was derived relating dynamic contact angle to velocity. The coefficients in this equation, however, were not related to any specific physical properties of the liquid and solid constituting the system, and the equation could therefore not be used to predict the behavior of unexplored liquid-solid combinations.

The present work was undertaken with four separate objectives in mind. The first objective was to study the contact angle-velocity relationship of selected systems in which the static contact angle was greater than zero but less than 90 degrees. The solid surfaces in these systems were to be smooth. The second was to determine the effect of surface roughness on the contact angle-velocity relationship among selected systems having a zero static contact angle. The third was to determine the effect of surface roughness on the contact angle-velocity relationship among systems having the non-zero static contact angle. The final objective was to develop a theoretical basis for relating dynamic contact angle behavior to the physical or chemical properties of the system's components, so that equations might be developed which could predict the dynamic contact angle behavior of unexplored systems. All the data gathered in this study and the previous study (ref. 1) would be used in developing and testing such equations.

## BACKGROUND

A rational explanation of the contact angle-velocity relationship in terms of material properties of the system might presumably be derived in an inductive manner by first finding an empirical equation expressing the functional relationship between the two variables, and then relating the coefficients of this equation to the pertinent physical properties. This approach, taken in previous work (ref. 1) resulted in the equation:

$$\theta_d = a \cdot \tanh cV + d \cdot V^{1/3} \qquad (1)$$

For this equation to have any theoretical significance the coefficients a, c and d should themselves be relatable to physical properties which affect the $\theta$-V relationship. No attempt to express a, c and d in terms of such physical properties was made at that time because no theoretical guide was developed as to what the significant properties and their relationships might be. The functional form of equation 1 was purely empirical, and no serious attempt was made to correlate it with any theoretical model of dynamic contact angle formation.

Our present approach has involved deduction as well as induction. The first step was to develop (or adopt from the literature) models of contact angle formation, using the parameters most likely to be involved.

### Definitions and Qualitative Considerations

If we bring a mass of liquid of arbitrary initial shape into contact with a solid surface of arbitrary configuration, the liquid-vapor interface along the three phase line of contact (the LSV line) will tilt or tend to tilt until the equilibrium contact angle $\theta_{eq}$ is reached. At the same time the LV interface will tend to adjust itself to a state of constant curvature and minimum area compatible with the constraints of the system. This situation is illustrated by the behavior of a drop of liquid on touching a flat solid surface as shown in Figure 1, a-c: In a the drop has very recently touched the surface and $\theta$ is still almost 180°. The LSV line is moving radially outward. In b, some time later, $\theta$ has become smaller; and the LSV line is still moving outward but it is moving more slowly than in a. In c

the system has come to equilibrium, the LSV line has stopped moving and $\theta$ has reached its equilibrium value. The angles $\theta_a$ and $\theta_b$ formed between the LV and SL interfaces while the LSV line is moving along the solid surface are dynamic contact angles, for which we shall use the general symbol $\theta_d$.

In Figure 1 the LV interface is shown at all three stages in its equilibrium constant-curvature minimum-energy shape, that of a spherical zone. This is of course possible if the outward motion of the LSV line is very slow, and the rate at which the LV interface can readjust to constant curvature after distortion is rapid. Such will be the case if the surface tension is high and the viscosity low. In general, however, the LV interface will not be in a state of constant curvature while liquid is in motion at the LSV line. Consider, for example, the representation of a wire running through a liquid shown in Figure 2. In 2a the system is at rest. The pressure differential across the LV interface is the same at all points, and this is equivalent to constant curvature if gravity effects are negligible. In the subsequent discussion we shall assume that gravity effects are negligible and use constant curvature to mean constant pressure difference across the interface. The LSV line is at an equilibrium level P above the bulk liquid surface Q, and the contact angle at LSV is at its equilibrium $\theta_{eq}$ (illustrated as equal to zero). In 2b we have started to move the filament S downward into the bulk liquid, and can visualize a hypothetical transitory situation in which (assuming no slippage at the SL interface) the LV surface has been distorted as shown to produce a high pressure region at H. The liquid accordingly flows toward the SL interface at the LSV line (Figure 2b) and prevents the contact angle from increasing indefinitely. A steady state is reached in which liquid removed from the LSV region by the moving SL interface is replenished by liquid forced in by the Laplacian pressure differential, the Laplacian pressure at each point on the surface being expressed by the equation:

$$P_1 - P_2 = \gamma_{LV}\left(\frac{1}{R_1} + \frac{1}{R_2}\right) \qquad (2)$$

where $R_1$ and $R_2$ are the principal radii of curvature of the interface. The LV interface remains in a slightly distorted configuration, sustained by

the viscosity of the liquid and opposed by the LV surface tension, as shown in 2c, and the contact angle comes to a steady value, $\theta_d$, which is greater than $\theta_{eq}$.

In the system of Figure 1 the only forces tending to change $\theta_d$ are molecular forces acting in the LSV line. In Figure 2 these molecular forces are supplemented by the hydrodynamic force of the distorted LV interface, which is dependent on the motion of the filament through the bulk liquid. The two systems accordingly differ in an important and fundamental manner. We shall refer to one as "self-spreading," and the other as "forced spreading."

The driving forces in self-spreading can be analyzed in terms of the familiar Young's equation picture, Figure 3. Young's equation states that at equilibrium, with all phases (including the surface phases) mutually saturated:

$$\gamma_{SV} = \gamma_{SL} + \gamma_{LV} \cos\theta_{eq} \tag{3}$$

Molecules in the LSV line (which may be regarded as a persistent statistical entity even though individual molecules are constantly moving in and out of the region) are constrained to move in the plane of the solid surface. The SV interface purportedly exerts a pull of $\gamma_{SV}$ dynes per centimeter on these LSV molecules. This pull is directly opposed by the pull of the SL interfacial layer, and by the component of $\gamma_{LV}$ in the SL-SV plane. At equilibrium the resultant of the three pulls is zero. For a system in which $\gamma_{SV}$ and $\gamma_{SL}$ have attained their equilibrium value but $\theta_d > \theta_{eq}$ the force on 1 cm of LSV line is potentially equal to:

$$\gamma_{LV}\left(\cos\theta_{eq} - \cos\theta_d\right) \tag{3a}$$

The forces which oppose motion of the LSV line are viscous in nature. Viscosity at the SL interface (for all liquids) and at the LV interface (for multicomponent liquids) may, however, differ greatly from ordinary bulk viscosity. The effective retarding force in the thin portions of liquid near the LSV line, particularly in a system of zero $\theta_{eq}$, may therefore differ from that calculated on the basis of bulk viscosity only.

Work by previous investigators (documented in a subsequent section of this report) presents the picture of self-spreading illustrated in Figure 4, which shows one profile of a spreading drop. In 4a, shortly after the drop has been touched to the solid, the strong pull of the SV interface has caused a thin layer of liquid Y to move out from the bulk of the liquid. Since the effective pull of SV cannot extend above the SV plane more than a very few molecular diameters the layer Y is quite thin and is probably not fluid in the dimension normal to the solid plane. Following Y is a region of liquid B sufficiently thick to have complete liquid properties. Following B is the bulk region E of normally behaving liquid. The layer Y, in the range of 1000 Å or less thick, has been observed and the region B has also been observed in drops spreading on smooth flat plates (ref. 2). When the system reaches equilibrium the region B disappears, merging into E. It is not known if Y persists or, if so, how far along the solid surface it extends.

Experimentally it is difficult to define a contact angle in the a and b stages of spreading. The layer Y is quite invisible in profile. The layer B supposedly has a thickness in the range of 1-2 microns and is equally invisible in conventional experimental systems. The "dynamic contact angle" we measure in a system of this type is the angle formed between the solid surface and the projection of the LV interface above B, as shown in Figure 4b.

No picture of forced spreading, analogous to the above picture of self-spreading, has been presented in the literature of surface chemistry. Forced spreading in the high velocity regime is studied in hydraulics under the general heading of "open channel surging." In particular the problem "propagation of a surge on a dry bed" deals with an LSV line moving across a dry solid surface impelled by pressure. The parameters that are considered, however, do not include the angle formed between the flat solid surface and the advancing wall of water. In the usual treatment this angle is assumed to be 90° at the start of the flow and (ideally) to remain constant.

## Pertinent Prior Studies of Spreading Rates and Dynamic Contact Angles

The more important studies of dynamic contact angles, pertinent to the present problem may be summarized as follows:

1. Hardy (ref. 3) studied the spreading of liquid droplets on solids from a qualitative point of view. He demonstrated that the visible spreading of a droplet on a solid is preceded by the spreading of an invisibly thin (less than one micron) "primary film," and that this film forms much more rapidly when the spreading liquid is volatile. He pointed out the very important role that the vapor phase plays in spreading on solids.

2. Bangham and Saweris (ref. 4) studied the spreading of various liquids on cleaved mica surfaces, thereby eliminating any possible artifacts due to roughness. Among many careful and extensive observations they found the behavior of liquid drops as regards spreading to depend on the structure and properties of the adsorbed film at the solid/gas interface. On mica the films formed by their organic vapors were polymolecular except at low pressure, and by the use of supersaturated vapors they could be built up to Newton's colour thickness before nuclei of condensation for the bulk liquids appeared. The effect of the surface was appreciable, therefore, not merely at molecular, but also at colloidal distances. Non-spreading liquids could generally be made to spread under the influence of the vapor of a suitably chosen second component.

3. The first quantitative measurements of spreading rates were made by Bascom et al (ref. 5). They concentrated on the slower regimes of spreading, corresponding to very low values of the dynamic contact angle. They made no attempt to measure a macroscopically visible contact angle such as we have attempted to define in the introductory discussion above, but they did study the geometrical form or profile of the LV interface at the advancing front, and measured the rate of advance of the front. They operated largely with liquids of low volatility. Their conclusions, verbatim, are as follows:

"A study by interference microscopy and ellipsometry shows that the spontaneous spreading of nonpolar liquids on smooth, clean metal surfaces is characterized by the advance from the bulk liquid of a primary film less than 1000 Å thick, usually followed by a thicker secondary film. The movement of the secondary film results from a surface tension gradient across the transition zone between the primary and secondary films. This gradient

is produced by the unequal evaporative depletion from these two regions of a volatile contaminant having a lower surface tension. If the volatile contaminant has a higher surface tension than the main component, the gradient is reversed, and the liquid recedes. Removal of the volatile constituents eliminates the secondary but not the primary spreading. Liquid may also spread by capillary flow in microscratches."

Aside from their general confirmation of Bangham and of Hardy, that pure liquids in their saturated vapor spread very slowly, their study of the effect of surface roughness is of great interest. Surface scratches across the path of flow decrease the spreading rate but scratches parallel to the path increase it. The rate on a polished surface is half way between the two, as shown in Figure 5. On this basis we should expect that the rate of spreading over a randomly rough surface would be the same as over a polished surface. Bascom et al. also demonstrated that the surface energy of the substrate has no effect on the spreading rate of the secondary film (the B-E region in Figure 4) provided the equilibrium contact angle of the system is zero, and that the macroscopically observable $\theta_d$ is a projection as shown in Figure 4b.

4. A group of three recent papers by Schonhorn et al. (ref. 6), Newman et al. (ref. 7) and Yin (ref. 8) all deal with the spreading of droplets of molten polymers on smooth surfaces. The polymers studied were quite viscous at the operating temperatures. In a typical run, starting with droplets of about 5 mg having a basal radius of about 1 mm, it took approximately 1500 seconds for the drop to spread radially a distance of 0.5 mm. In this very slow regime the droplet maintained the form of a spherical segment. The driving force for the spreading was taken to be an "instantaneous spreading coefficient." When $\theta_{eq} = 0$ this coefficient is:

$$S_0 = \gamma_{SV} - \gamma_{SL} - \gamma_{LV} \cos\theta_d \qquad (4)$$

The sole force resisting the spreading was taken to be the bulk viscosity of the liquid. On this basis it was found that all the data could be fitted onto one master curve using the scaling factor $\gamma_{LV}/R_o\eta$

where $\gamma_{LV}$ is the surface tension of the liquid, $\eta$ is the viscosity and $R_o$ (the basal radius of the hemispherical droplet sitting on the test surface) is a measure of the drop size. These papers deal with self-spreading entirely, and the authors state explicitly that the droplets maintain a spherical LV interface throughout the spreading process.

5. Rose and Heins (ref. 9) made the first study of contact angle vs. liquid velocity under the conditions we call forced spreading. They pushed slugs of liquid through a glass tube by means of air pressure, as shown in Figure 6, and observed both the advancing and receding contact angles as a function of liquid velocity. Since they worked only with systems in which $\theta_{eq} = 0$, the receding contact angle remained zero but the advancing angle did increase with increasing velocity. Their data show considerable scatter but they did get an apparently linear relationship between $\cos\theta_d$ and velocity in the range of .015-.2 cm/sec. Within this velocity range the contact angle of a mineral oil they were using (viscosity = 105 cp and surface tension = 30.1 dynes/cm) went from 30° to 63°. It is of interest that although the $\theta_{eq}$ of this oil on glass was zero the measured $\theta_d$ at .015 cm/sec was an unexpectedly high 30°.

6. Elliott and Riddiford (refs. 10, 11) studied the forced spreading of water on polyethylene and siliconed glass surfaces. The static advancing contact angles in these systems was 100° and 105° respectively. They used a technique in which liquid or air was held between two parallel glass plates and an air or liquid bubble was forced in from a syringe to form an LSV boundary line which could be moved in either direction at a controlled rate. They plotted contact angle vs. interfacial velocity in the velocity range zero to about 18 mm/min (0.3 cm/sec). Their lowest measured velocity was about 0.5 mm/min (.0008 cm/sec). Their results are shown in Figures 7 and 8. At very low velocities $\theta_d$ remained equal to $\theta_{eq}$. At a certain critical velocity the angle started to increase rapidly then leveled off.

The authors ascribe this behavior to a molecular relaxation phenomenon occurring at the advancing three phase boundary line. It takes a finite

time (the relaxation time) for the molecules of the advancing liquid to assume their equilibrium state on the solid surface. [It is generally recognized in surface chemistry that in dynamic systems the instantaneous values of the interfacial energies may differ considerably from their equilibrium values. If the liquid consists of a pure single component $\gamma_{LV}$ (dynamic) will be identical with $\gamma_{LV}$ (static) except possibly at very high velocities. $\gamma_{SV}$ (dynamic) will be higher than $\gamma_{SV}$ (static) unless SV interface has been presaturated with the vapor of the oncoming liquid. At high velocities $\gamma_{SL}$ (dynamic) can exceed $\gamma_{SL}$ (static) if the speed measured in seconds to traverse one molecular diameter exceeds the relaxation time (in seconds) of the liquid molecules.] A "natural" displacement velocity, $V_n$ can therefore be defined, according to ideas previously proposed by Hansen and Miotto (ref. 12) as:

$$V_n = \frac{L}{\tau} \tag{5}$$

where L is the thickness of the advancing LSV line and $\tau$ is the relaxation time. If V, the rate of advance of the LSV line, is much less than $V_n$ the dynamic contact angle will be equal to the static equilibrium (advancing) angle. As V increases and becomes appreciable relative to $V_n$ the state of the liquid in the LSV line is intermediate between that of bulk liquid and that of fully sorbed liquid and the contact angle is correspondingly higher than $\theta_{eq}$. At a sufficiently high velocity the residence time of the LSV line becomes so short that the liquid in the line has no chance at all to depart from its bulk state.

Elliott and Riddiford also observed another important phenomena illustrated in Figure 9. If the LSV front is advancing at a rate >1 mm/min and the drive is cut off the angle relaxes back to its equilibrium value in a relatively short time. Further decreases in angle over a longer period are attributed to slower solid-liquid interactions.

7. Friz (ref. 13) made a theoretical hydrodynamic analysis of a slug of liquid being pushed through a tube (the same system considered by Rose and Heins) and derived an equation for the shape of the liquid front and the apparent contact angle. Friz assumed that the wall of the tube was already wet with a thin layer of liquid (thickness = $\delta$, an important

parameter in his derivation). He also made several other explicitly stated assumptions which simplify the calculations but impair the accuracy of the system. Not the least of these was neglecting the radial curvature of the conduit, and developing the system in two dimensions rather than in three. His picture of the dynamic contact angle as an asymptotic limit to the actual LV profile is very satisfying, however. His equation for the dynamic contact angle is:

$$\tan\theta_d = 3.4 \sqrt[3]{\frac{u_0 \eta}{\gamma_{LV}}} \qquad (6)$$

where $\theta_d$ is the dynamic contact angle, $u_o$ is the forward velocity of the liquid, $\eta$ is viscosity and $\gamma_{LV}$ surface tension.

Friz made some experimental observations in which the profile of the advancing front checked his theoretical calculations qualitatively, but were off quantitatively by a factor of 3. He makes a tentative suggestion that the value of $\eta$ in thin layers may differ from that in bulk, and that this difference may account for the discrepancy. He also notes explicitly that $\theta_d$ advancing, and the shape of the advancing LV interface, may differ widely from his calculated values if the SV interface ahead of the LSV line is dry (i.e. if $\delta$ gets so small that the layer no longer behaves like a liquid).

Coney and Masica (ref. 14) tested Friz' theory experimentally. They measured both dynamic contact angle and interfacial shape as a function of interface velocity and liquid properties, using rectangular glass tubing which had been prewetted. The experiments were conducted in a weightless environment, and all the liquids used had zero static contact angles on the glass. Velocities ranged from 1.4 to 28 cm/sec; liquid surface tensions from 16.6 to 24.4 dynes/cm; and liquid viscosities from 0.56 to 6.7 centipoises. They found that the theory adequately predicted the contact angle dependence on interface velocity and liquid properties. Qualitative agreement was obtained between the theoretical and experimental interfacial shapes.

8. Cherry and Holmes, (ref. 15) studied the spreading of molten droplets of polyethylene on stainless steel at 150°C, and confirmed the results

of previous investigators. Their theoretical treatment is based on the idea that the activation energy for flow is the rate-controlling factor in spreading. Using Eyring's theory of absolute reaction rates they arrive at the equation:

$$\frac{d\cos\theta_d}{dt} = c\cdot\cos\theta_{eq}\cdot a\cdot e^{-ct} \tag{7}$$

where $c = \gamma_{LV}x^2y/\eta V_h$ where $V_h$ is the volume of the moving hydrodynamic unit, y is the dimension of the hydrodynamic unit in the direction of movement and x is the distance between sites. On this basis $\gamma_{LV}/\eta$ is the controlling factor. They note, however, that with low viscosity liquids surface-liquid interactions may become important. Equation 7 can be rearranged (ref. 16) to the form:

$$V = \frac{\gamma_{LV}}{\eta}\cdot\frac{x^2y}{V_h}\left(\cos\theta_{eq} - \cos\theta_d\right) \tag{7a}$$

so that a plot of V against ($\cos\theta_{eq}$-$\cos\theta_d$) would be linear.

9. Blake and Haynes (ref. 16) present by far the most succinct and convincing theoretical treatment of dynamic contact angles. Using the theory of absolute reaction rates they picture the essential motion to be a sliding of the molecules along the solid surface from the liquid to the vapor side of the LSV line. The work expended in causing the flow is:

$$W = \gamma_{LV}\left(\cos\theta_{eq} - \cos\theta_d\right) \tag{8}$$

and this is used to raise or lower the activation energy for forward or reverse molecular migration along the solid surface. Blake and Haynes thus regard the retarding force as an <u>interfacial</u> viscosity, in contrast to the bulk viscosity used by the other investigators cited. The concept of interfacial viscosity and the fact that it is in general different from the bulk viscosity are well established in surface thermodynamics. Their final equations are:

$$V = 2K\lambda\sinh\left[\frac{\gamma_{LV}}{\Delta nkT}\left(\cos\theta_{eq} - \cos\theta_d\right)\right] \tag{9}$$

$$V = \frac{2K\lambda\gamma_{LV}}{\Delta nkT}\left(\cos\theta_{eq} - \cos\theta_d\right) \qquad (10)$$

$$V = K\lambda \exp\left[\frac{\gamma_{LV}}{\Delta nkT}\left(\cos\theta_{eq} - \cos\theta_d\right)\right] \qquad (11)$$

where V is the forward velocity of the liquid, K is number of molecular displacements occurring per unit time per unit length of the LSV line, $\lambda$ is the average distance between sites on the solid surface, $\Delta n$ is surface concentration of sites, and the other symbols have their usual significance. Equation 9 is the master equation, valid over the whole velocity range. From the mathematical properties of the hyperbolic sine function it follows that equation 10 becomes approximately valid if the argument of sinh (i.e the expression in brackets) in equation 9 is small. Equation 11 becomes approximately valid if the argument of sinh in equation 9 is large. If we designate $(\cos\theta_{eq}-\cos\theta_d)$ by $\Delta\cos$, plots of either $\Delta\cos$ vs. V or $\cos\theta_d$ vs. V would be linear in the range where equation 10 was valid, and they would be exponential (linear on semi-log paper) in the range where equation 11 was valid.

Blake and Haynes obtained experimental data for the system benzene-water-siliconed glass, using cylindrical capillary tubes of .2mm diameter and velocities in the range of zero to 1 cm/sec (600 mm/min). This is a system similar to that of Rose and Heins. Their plots of $\cos\theta_d$ vs. velocity on semi-log paper were linear, as shown in Figure 10, indicating that equation 11 was governing in this system. They point out that their treatment differs from Cherry and Holmes' in using surface flow rather than bulk flow (viscosity) parameters. They also point out that their derivation is valid only on the basis of a single-valued $\theta_{eq}$. Thus systems that show true contact angle hysteresis, such as the systems of Elliott and Riddiford, may not necessarily behave according to equation 9.

Summarizing Remarks

Summarizing the literature, it appears that aside from Friz all workers regard $\gamma_{LV}(\Delta\cos)$ as the sole driving force tending to advance the LSV line. In Friz' treatment the movement is a surge, with the driving force an exterior pressure. All workers except Friz and Blake-Haynes regard the bulk viscosity $\eta$ of the liquid as the sole resistance force. Friz' resistance force is a function of both $\eta$ and $\gamma_{LV}$. Blake and Haynes' resistance force can be regarded as a solid-liquid interfacial viscosity or resistance to movement along the solid surface through the LSV line. It is dependent on the properties of the SL and SV interfaces as well as those of the bulk liquid.

The raw data of the experiments described above, as well as the experiments hereinafter reported, are in the form of tables of $\theta_d$ vs. V. To find out which if any of the three major theories is applicable, and if so the velocity range within which it is applicable, the data may be plotted in three different ways:

1. As $\Delta\cos$ vs. V. This is referred to as a cosine plot. If the cosine plot is linear over any substantial range it might indicate a Yin (ref. 8 ) or Cherry-Holmes (ref. 15) type of relationship. It might also indicate a Blake-Haynes (ref. 16) type of relationship in which the argument of the sinh function is small as in equation 10. If the cosine plot is curved, and has the general form of a sinh function, the numerical values of the coefficients in equation 9 can be estimated, and from them values of K, $\lambda$ and $\Delta n$ can be derived. These derived values can then be compared for magnitude with physically reasonable values of K, $\lambda$ and $\Delta n$. A close match between the values derived from the experimental data and values known to be reasonable would constitute a strong indication that the Blake-Haynes mechanism is operative, at least over the velocity range studied.

2. As a plot of $\Delta\cos$ vs. log V. This is referred to as a Haynes plot. If it is linear it would indicate a Blake-Haynes mechanism in which the argument of the sinh function is large, as in equation 11.

3. As a plot of log tan$\theta_d$ vs. log $\eta/\gamma_{LV}$ V. This is referred to as a Friz plot. If it is linear it would suggest a Friz (ref. 13) mechanism, as described by equation 6. Equation 6 requires that such a plot have a slope of .33, and it is also obvious that the equation cannot be valid for values of $\theta_d$ approaching 90°. The mathematical form of the relationship (tan$\theta_d$ being a power function of V) would nevertheless still suggest a physical situation similar to that postulated by Friz, i.e. an outside pressure as the driving force, with viscosity as one resistance force and a continuously increasing back pressure against the advancing liquid front as a second resistance force. Mere linearity of a Friz plot of experimental data on $\theta_d$ vs. V would not necessarily indicate, however, that a Friz type of mechanism was veritably applicable. The same data would also give a linear Haynes plot for values of $\theta_d$ between about 38° and 73°. Within this range the relationship between the cosine of the angle and the log tangent of the angle is very nearly linear.

## EXPERIMENTAL

The relationship between $\theta_d$ and V was studied for the ten liquid-solid systems designated in Table I by either XY or Y. This distinguishes them from the previously studied systems (ref. 1) which are designated by X. The five systems designated by Y are those for which the static contact angle $\theta_{eq}$ is greater than zero but less than 90°. In these systems new data were developed for the solid in both the smooth state and at three different degrees of roughness. The five systems designated XY had previously been studied in the smooth state only and these prior smooth state data were used in the present analysis. New data were developed for these systems at three different degrees of roughness. All the new data extended into a much lower velocity range than the old. The properties of the liquids used, and the values of the static contact angles of all the systems, are given in Table II.

The apparatus and methods of measuring both $\theta_d$ and V were the same as described previously (ref. 1). The apparatus was very slightly modified to enable velocities as low as .0002 cm/sec to be measured. The solids were used in the form of cylindrical filaments 20 mils in diameter. The cleaning

and manipulative procedures were the same as described previously. The liquids were the purest grade available commercially.

Preparation of Roughened Specimens

Roughened filaments were prepared by sandblasting. The filament from a supply spool was passed upward through the sandblasting box, receiving the blast from three nozzles placed symmetrically around the filament. The filaments were examined microscopically to check that the roughening was complete and uniform. Usually one pass was sufficient to accomplish this result. The three different degrees of roughness were obtained by using three different sizes of carborundum grit; #120, #180 and #240. The appearance of the specimens roughened by any one grit varied very little with the material, i.e. the #120 roughened steel, nylon, PMMA and Teflon all appeared to have about the same roughness, and all were rougher than the #180 specimens. Figure 18 shows the appearance of the smooth and roughened stainless steel wires under the scanning electron microscope at 200X magnification. Direct measurements of roughness could not be made on the filaments. To estimate the roughness flat specimens of each material were sandblasted in the same manner as the filaments, and their appearance under the microscope was checked against that of the correspondingly roughened filaments. The "center line average deviation" roughness of flat specimens of the PMMA, nylon and stainless steel was measured by a Taylor-Hobson "Talysurf" machine fitted with an automatic integrator. The roughness of the #120 specimens was 26-35 microinches; #180 specimens 20-23 microinches; and #240 specimens 11-15 microinches. The smooth specimens had a roughness near the resolution limit of the instrument, about 2 microinches. The traces were quite uniform with regard to direction along the specimen, indicating well-randomized roughening. Precise measurements could not be obtained on the Teflon due to its softness.

Precision and Accuracy of the Contact Angle Measurements

Although the precision of the measurements of $\theta_d$ was reasonably good, about $\pm$ 1°, the accuracy, which was not determined, was probably poorer. This was due largely to vibration in the system. A run made with the hexadecane-smooth nylon system at a velocity in the range of 20 cm/sec was

analyzed for error due to vibration. At this high velocity it was found that $\theta_d$ ranged from about 78-81° with a frequency of about 30 per second, and that from time to time the range became as great as 70-87° The range was usually lower, however, particularly at lower velocities and angles. A related source of inaccuracy was the procedure for selecting the pictures for angle measurement. A strip of film was selected in which the velocity (as shown on the tachometer or calculated from the turns of the marked gear wheel) remained constant. This strip might be well over 100 frames long. Along this strip five frames were selected, ten frames apart, and the angle was measured on both sides of the wire. The ten measurements thus obtained were averaged to give the value of $\theta_d$ shown in the tables. In a set of ten a narrow range of values would be 2°, a wide range of values might be as high as 9°. The selection was arbitrary, and standard deviations were not calculated. The accuracy of the measurements is therefore based on the large number of readings taken and averaged. It is difficult to estimate how far any single tabulated value of an angle may be from the ideal true value. After analysis of all factors involved, however, we believe that such deviations will seldom be more than 5 degrees.

Results

Data for the ten different solid-liquid combinations studied are presented in Tables III-XII. As noted above, data for smooth surfaces of the five systems marked XY in Table I are taken from previous work (ref. 1). All other data is from the present study. In some of the tables for the five systems having a $\theta_{eq}$ greater than zero there is a difference between the values of $\theta$ at zero velocity depending on the roughness. This is because the measurements were made without adjusting the wire to read the equilibrium value. Roughened surfaces produce contact angle hysteresis and static contact angles measured without adjustment are haphazardly specious. Dynamic angles in such systems are not subject to this error. The true values of $\theta_{eq}$ are those given in Table II.

For purposes of analysis the data were arranged and diagramed in the form of cosine plots, Haynes plots and Friz plots, each of which will be used as appropriate in the following discussion of results.

## DISCUSSION OF RESULTS

### Effect of Magnitude of the Static Contact Angle

Whether the static equilibrium contact angle is zero or positive appears to have no effect on the form of the $\theta_d$ vs V relationship. Figure 11 shows Haynes Plots of three positive angle systems and two representative zero angle systems, all at the same degree of roughening, #240 grit. For reasons given in a following section on Theory Development the Haynes plot is considered the most revealing way of presenting and comparing the data. Ordering the systems with regard to $\theta_{eq}$ and slope, it is evident that no correlation exists. There is no theoretical reason why any functional relationship should exist between $\theta_{eq}$ and the form of the $\theta_d$-V curves. It is noteworthy that the geometric form of all the curves, however, is the same. Regardless of the static contact angle the LSV line is advancing over a dry surface, and the three phase interfaces that determine the force balance are all of the same type.

### Effect of Roughening and Roughness

The roughened surfaces used in the present studies were produced by blasting with grit of three different sizes but of the same chemical composition. The blasting destroys the old surface of the substrate and exposes a new surface which may or may not differ in physicochemical properties from the old one. Presumably the three new surfaces formed by the three different sizes of grit will have identical physicochemical properties. If we wish to ascertain the effect of roughness (i.e. of surface geometry alone) on the $\theta_d$-V relationship comparisons should be made of the three roughened surfaces with one another. If, on the other hand, we wish to ascertain the effect of roughening (i.e. of changing the original surface by abrading and disrupting it) comparison should be made between the original smooth surface and any of the three roughened surfaces.

Comparisons of one $\theta_d$ vs. V function with another is conveniently made by means of the Haynes plot. Key features of the Haynes plot, in the regions pertinent to these studies, are the slope of the low velocity leg (slow side slope), the slope of the high velocity leg (fast side slope) and the velocity $V_c$ at which the characteristic transition between the two occurs. These are given in Tables XIII - XVI. Referring first to Table XIII, in each of the three stainless steel systems the three roughened specimens show no significant differences among themselves, but they all appear to differ from the corresponding smooth specimen, at least in values for fast side slope which was the only parameter evaluated in the smooth systems. This would suggest that blasting changed the physicochemical character of the stainless steel surface, but that degree of roughness has little if any effect on the $\theta_d$ vs. V relationship. Haynes plots of the four stainless steel-hexadecane systems are shown in Figure 12.

Data for the nylon systems are given in Table XIV. The nylon-water systems are anomalous, presumably because water swells nylon to a considerable extent and thereby alters the surface profoundly as it passes onto it. The other three liquids all give systems in which neither the degree of roughness nor the transition from smooth to abraded surface appears to change the $\theta_d$ vs. V relationship significantly. The value for $V_c$ in the alpha bromonaphthalene-#240 grit system seems high. Figures 13 and 14 show Haynes plots of the nylon-methylene iodide systems and the nylon-hexane systems respectively. The latter are of the type described by Elliott and Riddiford (refs. 10, 11), in which $\theta_d = \theta_{eq}$ below a certain critical velocity.

The PMMA-hexane systems (Table XV) may show an anomalously low value for the #120 roughened fast side slope. In view of the reasonably well matching values of $V_c$ and of the slow side slopes this may be due to experimental error. In the Teflon systems (Table XVI) it is evident that degree of roughness has no significant effect. It is difficult to tell whether the effect accompanying abrasion of the surface in these systems is significant or not.

## Development of the Theory of the $\theta_d$-V Relationship

Data for all the systems listed in Table I were graphed in the form of cosine plots, Haynes plots and Friz plots. The systems designated X in Table I gave what appeared to be approximate straight lines in all three methods of plotting. This was due, however, to the fact that the data were confined to the relatively high velocity ranges. Those systems (designated Y) for which data were available into the low velocity range gave quite a different picture. The nylon-hexane and stainless steel-hexane systems showed displacements of the curves at a critical velocity, below which $\theta_d$ remained equal to $\theta_{eq}$. This is the behavior described by Elliott and Riddiford (refs. 10, 11) and shown in Figures 7 and 8. It is illustrated for the nylon-hexane systems in Figure 14, which also shows (curve a) that the high velocity data misses the characteristic break region and suggests a linear relationship. The remaining systems showed the following typical behavior:

The cosine plots were curved, and had the general form of an exponential or hyperbolic sine curve. Typical plots are shown in Figures 15 and 15a. Attempts to find coefficients which would fit equation 9 to these curves were reasonably successful so far as the lower velocity ranges were concerned. At higher velocities the coefficients had to be changed markedly, indicating that equation 9 was not valid over the whole velocity range. The shape of the curves indicated that equations 10 or 7a could not be valid, at least in the low velocity range.

The Friz plots all departed from linearity, as expected, as $\theta_d$ approached 90°. Below this region the typical Friz plot had the general form of two intersecting straight lines, as shown in Figure 16a, or an upward trending curve (Figure 16b) which might be interpreted as two linear regions with a gradual rather than a sharp intersection.

The Haynes plots typically showed two essentially linear regions intersecting more or less sharply as shown in Figures 11 and 13, the slope ($\Delta\Delta\cos/\Delta \log V$) of the fast side being greater than that of the slow side. The similarity between the Friz and Haynes plots in certain velocity ranges is shown by comparing Figures 16a and 17.

This graphic behavior strongly suggested that at least two mechanisms were governing the $\theta_d$-V relationship, one of which predominated at lower and the other at higher velocities. If this were the case, and the two mechanisms were the Blake-Haynes (according to equation 11) and the Friz, we would expect the Blake-Haynes to govern at lower velocities and the Friz at higher velocities. To test this hypothesis the fast side slopes and the slow side slopes of the Blake-Haynes plots (Tables XIII-XVI) were used separately to evaluate $\Delta n$ and $\lambda$, using the Blake-Haynes method (ref. 16) which starts with equation 11. The values of $\lambda$ calculated from fast side slopes are of the order of 5-10 Å, which is considered small and less in accord with current theories of the liquid state than the values of 15-30 Å calculated from slow side slopes. This supports the hypothesis that in the low velocity region the Blake-Haynes mechanism predominates. Further support comes when K in equation 11 is evaluated, from $\lambda$ and the intercept of the slow side leg with the $\Delta\cos = 0$ axis. Substituting the values of K, $\Delta n$ and $\lambda$ into equation 9 and plotting the curve, it is found to superpose the experimental curve of $\Delta\cos$ vs. V remarkably well in the low velocity region. The experimental curve in this region is thus shown to be sinh curve, in conformity with the Blake-Haynes theory. This is illustrated in Figures 15 and 15a.

In the higher velocity region, corresponding to the fast side legs of both the Haynes plots and the Friz plots, the data can be well represented by an equation having the form of equation 6, i.e.

$$\tan\theta_d = a\left(\frac{\eta V}{\gamma_{LV}}\right)^b \qquad (12)$$

This represents a surging motion in which the bulk fluidity $1/\eta$ rather than the interfacial fluidity $K\lambda$ is the governing parameter. Since the liquid surges onto a dry bed, and since the flow is superposed on a flow of the Blake-Haynes type the parameters a and b should differ from those of equation 6, and the scaling factor should be some unascertained combination of $K\lambda$, $\eta$ and $\gamma_{LV}$ rather than $\eta/\gamma_{LV}$.

In forced spreading the general form of the $\theta_d$-V relationship over the range from $\theta_d = \theta_{eq}$ to $\theta_d \rightarrow 90°$ may accordingly be described as follows:

At the lowest velocities there is a region in which $\theta_d = \theta_{eq}$. This region was observed experimentally in the present study only with systems in which hexane was the liquid (although there is a suggestion of similar behavior in the octane-#180 grit roughened Teflon system, Table V). Theoretically, according to the views of Hansen and Miotto (ref. 12) such a region should exist at sufficiently low velocities for all liquids.

Above this "Hansen-Miotto region" is a region in which the behavior described by Blake and Haynes, equation 9, predominates. In this region the major driving force is measured by $\gamma_{LV} \cdot \Delta\cos$ and the major retarding force is the solid-liquid interfacial viscosity measured by $1/K\lambda$. This parameter is a property of the solid-liquid pair, rather than of the liquid alone or the solid alone. The Blake-Haynes behavior is, of course, superposed on whatever Hansen-Miotto behavior may exist.

Above a relatively narrow critical velocity range a surging mode of flow of the type described by Friz (equations 6 and 12) becomes superposed on the Blake-Haynes mode, and becomes increasingly predominant as the velocity is further increased. In this Friz behavior the principal driving force is an external pressure, and the principal retarding force is the bulk viscosity $\eta$ of the liquid. The surface tension of the liquid $\gamma_{LV}$ plays a role in determining the shape of the advancing LV front and the magnitude of $\theta_d$.

## CONCLUSIONS

Based on the experimental results, and limiting the conclusions to the systems and velocity ranges studied, the following conclusions may be drawn:

1. The roughness of solid surfaces has no appreciable effect on the $\theta_d$-V relationship, provided the physicochemical character of the surfaces is the same. If the process of roughening alters the physicochemical character the $\theta_d$-V behavior of the roughened surface may differ from that of the smooth one.

2. There is no qualitative difference between the $\theta_d$-V behavior of systems in which $\theta_{eq}$ is zero and systems in which $\theta_{eq}$ is positive.

3. There appear to be three different modes according to which $\theta_d$ varies with V, each of which predominates in a different velocity range. In the lowest velocity range, with systems involving the low viscosity, low boiling, non-polar liquid hexane, $\theta_d$ was found equal to $\theta_{eq}$ (the Elliott-Riddiford or Hansen-Miotto mode). In the next higher velocity range, which extends to very low velocities for all other systems studied, the behavior described by equation 9 (the Blake-Haynes mode) predominates. At still higher velocities the behavior described by equation 12 (the Friz mode) becomes superposed on the Blake-Haynes mode, and eventually predominates up to the range where $\theta_d$ approaches 90° and equation 12 becomes inapplicable. In the Blake-Haynes mode the major force opposing advance of the liquid front is the solid-liquid interfacial viscosity. In the Friz mode it is the bulk viscosity of the liquid.

## LIST OF SYMBOLS

| | |
|---|---|
| $\theta$ | Contact angle (degrees) |
| $\theta_d$ | Dynamic contact angle (degrees) |
| $\theta_{eq}$ | Equilibrium contact angle (degrees) |
| $\Delta\cos$ | $\cos\theta_{eq} - \cos\theta_d$ |
| LSV | Liquid-solid-vapor line |
| LV | Liquid-vapor interface |
| SV | Solid-vapor interface |
| SL | Solid-liquid interface |
| $\gamma_{LV}$ | Liquid surface tension (dynes/cm) |
| $\gamma_{SV}$ | Solid-vapor interfacial tension (dynes/cm) |
| $\gamma_{SL}$ | Solid-liquid interfacial tension (dynes/cm) |
| $\eta$ | Viscosity (poises or centipoises) |
| $\Delta n$ | Surface concentration of sites ($cm^{-2}$) |
| $\lambda$ | Average distance between sites ($\mathring{A}$) |
| K | Number of molecular displacements per unit length of LSV per unit time |
| k | Boltzmann constant |
| T | Absolute temperature (° Kelvin) |
| $V_c$ | Characteristic transition velocity (cm/sec) |
| V | Interfacial velocity (cm/sec) |

## REFERENCES


1. A. H. Ellison and S. B. Tejada, NAS CR 72441, July 23, 1968.
2. W. B. Hardy, Collected Papers, Cambridge, 1936, p. 624ff.
3. W. B. Hardy, ibid; p. 711ff.
4. D. H. Bangham and Z. Saweris, Trans. Faraday Soc., 34, 554 (1938).
5. W. D. Bascom, R. L. Cottington and C. R. Singleterry, Advances in Chemistry Series, ACS, 43, 355.
6. H. Schonhorn, H. L. Frisch and T. W. Kwei, J. Applied Physics, 37, 4967 (1966).
7. H. Van Oene, Y. F. Chang and S. Newman, J. Adhesion, 1, 54 (1969).
8. T. P. Yin, J. Phys. Chem., 73, 2413 (1969).
9. W. Rose and R. W. Heins, J. Colloid Sci., 17, 39 (1962).
10. G. E. P. Elliot and A. C. Riddiford, Nature, No. 4843, 795 (August 25, 1962).
11. G. E. P. Elliot and A. C. Riddiford, J. Colloid Interface Sci., 23, 389 (1967).
12. R. S. Hansen and M. Miotto, J. Am. Chem. Soc., 79, 1765 (1957).
13. G. Friz, Z. fur Angw. Physik, 19, No. 4, 374 (1965).
14. T. A. Coney and W. J. Masica, NASA TND-5115 (1969).
15. B. W. Cherry and C. M. Holmes, J. Colloid Interface Sci., 29, 174 (1969).
16. T. D. Blake and J. M. Haynes, J. Colloid Interface Sci., 30, 421 (1969).
17. A. H. Ellison and W. A. Zisman, J. Phys. Chem., 58, 503 (1954).
18. T. Fort, Jr., Advances in Chemistry Series, ACS, 43, 302.

TABLE I

SYSTEMS STUDIED[a]

| Liquid | Solid | | | | | |
|---|---|---|---|---|---|---|
| | Stainless Steel | Titanium | Aluminum | Nylon | PMMA[b] | Teflon |
| Di(2-ethylhexyl)sebacate (DOS) | | | | | | Y |
| Diethylphthalate (DEP) | X | X | X | | | |
| Benzyl alcohol | X | | X | X | X | |
| Hexadecane | XY | X | X | X | X | |
| Isopropanol | X | X | | X | | |
| Absolute ethanol | XY | X | | X | | |
| Alpha bromonaphthalene | | | | Y | | |
| Freon TF | X | X | | X | | |
| Octane | | | | | | Y |
| Hexane | XY | | X | XY | XY | |
| Water | | | | Y | | |
| Methylene iodide | | | | Y | | |

a. X designates smooth solid only, data from ref. 1. XY designates data for smooth solid from ref. 1; data for roughened solid from present study. Y designates data for both smooth and roughened solid from present study.

b. Poly(methyl methacrylate).

TABLE II

PROPERTIES OF TEST LIQUIDS

| Liquid | Viscosity Centipoises | Surface Tension dynes/cm | $\eta/\gamma_{LV}$ | Static contact angle on smooth surface[a] | | | | | |
|---|---|---|---|---|---|---|---|---|---|
| | | | | Stainless Steel | Titanium | Aluminum | Nylon | PMMA | Teflon |
| Di(2-ethylhexyl)sebacate (DOS) | 25.0 | 31.2 | .808 | | | | | | 61 |
| Diethyl phthalate (DEP) | 10.10 | 37.5 | .270 | 0 | 0 | 0 | | | |
| Benzyl alcohol | 5.80 | 39.0 | .1485 | 0 | | 0 | 0 | 0 | |
| Hexadecane | 3.32 | 27.6 | .1205 | 0 | 0 | 0 | 0 | 0 | |
| Isopropanol | 2.22 | 21.7 | .1025 | 0 | 0 | | 0 | | |
| Absolute alcohol | 1.20 | 22.75 | .0529 | 0 | 0 | | 0 | | |
| Alpha bromonaphthalene | 2.3 | 44.6 | .0516 | | | | 16 | | |
| Freon TF | .694 | 19.0 | .0365 | 0 | 0 | | 0 | | |
| Octane | .542 | 21.8 | .0249 | | | | | | 26 |
| Hexane | .326 | 18.4 | .0180 | 0 | | | 0 | 0 | |
| Water | 1.00 | 72.0 | .0139 | | | | 70 | | |
| Methylene iodide | .50 | 50.7 | .00985 | | | | 41 | | |

a. Contact angle values measured experimentally. These check literature values (refs. 17, 18).

TABLE III

DYNAMIC CONTACT ANGLE-VELOCITY DATA FOR
DI(2-ETHYLHEXYL)SEBACATE ON TEFLON SURFACES

| Smooth | | #120 Grit | | #180 Grit | | #240 Grit | |
|---|---|---|---|---|---|---|---|
| Velocity cm/sec | Angle degrees | Velocity cm/sec | Angle degrees | Velocity cm/sec | Angle degrees | Velocity cm/sec | Angle degrees |
| 0 | 61 | 0 | 60 | 0 | 60 | 0 | 60 |
| 0.019 | 64 | 0.006 | 63 | 0.006 | 66 | 0.015 | 63 |
| 0.022 | 65 | 0.019 | 66 | 0.010 | 66 | 0.034 | 66 |
| 0.061 | 66 | 0.026 | 64 | 0.019 | 70 | 0.043 | 70 |
| 0.067 | 66 | 0.034 | 67 | 0.028 | 70 | 0.057 | 76 |
| 0.078 | 64 | 0.043 | 67 | 0.028 | 71 | 0.072 | 71 |
| 0.083 | 66 | 0.059 | 65 | 0.054 | 70 | 0.104 | 74 |
| 0.097 | 68 | 0.068 | 68 | 0.057 | 70 | 0.122 | 75 |
| 0.134 | 67 | 0.107 | 71 | 0.082 | 71 | 0.171 | 76 |
| 0.140 | 71 | 0.107 | 72 | 0.086 | 71 | 0.190 | 78 |
| 0.148 | 72 | 0.114 | 71 | 0.088 | 71 | 0.242 | 76 |
| 0.257 | 75 | 0.114 | 74 | 0.110 | 73 | 0.306 | 78 |
| 0.305 | 70 | 0.123 | 72 | 0.286 | 79 | 0.342 | 78 |
| 0.314 | 71 | 0.171 | 74 | 0.342 | 80 | 0.342 | 80 |
| 0.414 | 76 | 0.191 | 76 | 0.427 | 79 | 0.372 | 79 |
| 0.630 | 76 | 0.214 | 75 | 0.855 | 90 | 0.488 | 81 |
| 0.650 | 76 | 0.244 | 79 | | | 0.570 | 84 |
| 0.820 | 80 | 0.284 | 81 | | | 0.660 | 86 |
| 0.860 | 79 | 0.342 | 81 | | | 0.713 | 87 |
| 1.030 | 84 | 0.685 | 87 | | | 1.008 | 90 |
| | | 0.855 | 90 | | | | |

TABLE IV

DYNAMIC CONTACT ANGLE-VELOCITY DATA FOR
$\alpha$-BROMONAPHTHALENE ON NYLON SURFACES

| Smooth | | #120 Grit | | #180 Grit | | #240 Grit | |
|---|---|---|---|---|---|---|---|
| Velocity cm/sec | Angle degrees | Velocity cm/sec | Angle degrees | Velocity cm/sec | Angle degrees | Velocity cm/sec | Angle degrees |
| 0 | 16 | 0 | 22 | 0 | 22 | 0 | 22 |
| 0.022 | 23 | 0.042 | 26 | 0.043 | 23 | 0.029 | 23 |
| 0.065 | 30 | 0.060 | 26 | 0.054 | 24 | 0.046 | 22 |
| 0.10 | 33 | 0.095 | 27 | 0.090 | 26 | 0.058 | 24 |
| 0.139 | 35 | 0.114 | 24 | 0.153 | 34 | 0.086 | 25 |
| 0.335 | 40 | 0.155 | 30 | 0.214 | 36 | 0.098 | 27 |
| 0.52 | 48 | 0.182 | 36 | 0.245 | 43 | 0.127 | 30 |
| 0.70 | 54 | 0.238 | 41 | 0.286 | 45 | 0.168 | 32 |
| 0.97 | 61 | 0.329 | 43 | 0.342 | 48 | 0.202 | 32 |
| 1.08 | 61 | 0.364 | 49 | 0.373 | 50 | 0.745 | 40 |
| 1.54 | 62 | 0.745 | 53 | 0.450 | 53 | 1.863 | 53 |
| 1.88 | 66 | 1.863 | 66 | 1.677 | 62 | 2.795 | 62 |
| 2.26 | 70 | 2.795 | 70 | 2.795 | 65 | 3.727 | 73 |
| 2.47 | 70 | 3.913 | 72 | 3.727 | 73 | 5.031 | 74 |
| 3.20 | 71 | 4.565 | 75 | 4.658 | 80 | 5.683 | 75 |
| 3.35 | 72 | 6.242 | 82 | 5.776 | 81 | 6.894 | 76 |
| 3.70 | 74 | 6.801 | 84 | 6.708 | 84 | 7.453 | 77 |
| 4.10 | 76 | | | 7.267 | 86 | 9.317 | 87 |
| 5.93 | 82 | | | 7.640 | 88 | 10.150 | 90 |
| 5.50 | 83 | | | 7.826 | 90 | | |

TABLE V

DYNAMIC CONTACT ANGLE-VELOCITY DATA FOR
n-OCTANE ON TEFLON SURFACES

| Smooth | | #120 Grit | | #180 Grit | | #240 Grit | |
|---|---|---|---|---|---|---|---|
| Velocity cm/sec | Angle degrees | Velocity cm/sec | Angle degrees | Velocity cm/sec | Angle degrees | Velocity cm/sec | Angle degrees |
| 0 | 26 | 0 | 25 | 0 | 24 | 0 | 24 |
| 0.373 | 36 | 0.050 | 28 | 0.062 | 25 | 0.086 | 26 |
| 0.932 | 38 | 0.082 | 30 | 0.118 | 24 | 0.127 | 26 |
| 2.236 | 44 | 0.118 | 30 | 0.163 | 25 | 0.191 | 27 |
| 2.981 | 46 | 0.221 | 33 | 0.245 | 26 | 0.202 | 27 |
| 3.534 | 45 | 0.296 | 33 | 0.268 | 26 | 0.343 | 28 |
| 4.658 | 49 | 0.520 | 33 | 0.429 | 28 | 0.476 | 28 |
| 5.385 | 49 | 0.932 | 35 | 0.932 | 32 | 0.932 | 32 |
| 5.385 | 50 | 1.863 | 37 | 2.050 | 34 | 1.863 | 34 |
| 6.056 | 48 | 2.981 | 39 | 2.981 | 36 | 2.795 | 35 |
| 7.816 | 52 | 4.099 | 42 | 3.727 | 39 | 3.727 | 37 |
| 8.627 | 51 | 4.658 | 42 | 5.776 | 46 | 5.776 | 43 |
| 8.757 | 52 | 5.963 | 43 | 7.453 | 49 | 6.615 | 46 |
| 10.150 | 53 | 6.522 | 45 | 8.385 | 52 | 8.385 | 48 |
| 13.195 | 54 | 7.453 | 47 | 9.316 | 52 | 9.317 | 49 |
| 16.240 | 56 | 8.571 | 49 | 10.150 | 53 | 10.150 | 51 |
| 19.285 | 57 | 10.151 | 51 | 14.718 | 58 | 15.225 | 55 |
| 23.245 | 58 | 20.300 | 56 | 25.375 | 63 | 32.480 | 67 |
| 24.360 | 60 | 25.375 | 67 | | | 36.540 | 69 |
| 29.435 | 60 | 30.450 | 69 | | | | |
| 32.480 | 62 | 35.525 | 73 | | | | |
| 33.495 | 64 | 41.610 | 74 | | | | |
| 35.525 | 67 | | | | | | |
| 39.585 | 69 | | | | | | |
| 40.600 | 70 | | | | | | |
| 44.660 | 71 | | | | | | |
| 52.780 | 80 | | | | | | |

TABLE VI

DYNAMIC CONTACT ANGLE-VELOCITY DATA FOR WATER ON NYLON SURFACES

| Smooth | | #120 Grit | | #180 Grit | | #240 Grit | |
|---|---|---|---|---|---|---|---|
| Velocity cm/sec | Angle degrees | Velocity cm/sec | Angle degrees | Velocity cm/sec | Angle degrees | Velocity cm/sec | Angle degrees |
| 0 | 70 | 0 | 42 | 0 | 32 | 0 | 78 |
| 0.00044 | 74 | 0.006 | 66 | 0.0003 | 78 | 0.0005 | 78 |
| 0.00086 | 74 | 0.007 | 71 | 0.0004 | 77 | 0.0006 | 79 |
| 0.0018 | 74 | 0.009 | 82 | 0.0005 | 72 | 0.0007 | 78 |
| 0.0034 | 76 | 0.010 | 64 | 0.0005 | 75 | 0.0007 | 79 |
| 0.0038 | 77 | 0.010 | 73 | 0.0005 | 78 | 0.0008 | 79 |
| 0.0048 | 77 | 0.013 | 75 | 0.0006 | 74 | 0.0009 | 81 |
| 0.0099 | 79 | 0.014 | 74 | 0.0007 | 78 | 0.0009 | 83 |
| 0.012 | 80 | 0.014 | 77 | 0.0009 | 80 | 0.0011 | 79 |
| 0.020 | 82 | 0.015 | 80 | 0.0011 | 82 | 0.0011 | 83 |
| 0.027 | 83 | 0.016 | 77 | 0.0010 | 90 | | |
| 0.046 | 85 | 0.016 | 78 | 0.0013 | 90 | | |
| 0.060 | 85 | 0.022 | 82 | | | | |
| 0.063 | 84 | 0.020 | 79 | | | | |
| 0.120 | 87 | 0.030 | 86 | | | | |

TABLE VII

DYNAMIC CONTACT ANGLE-VELOCITY DATA FOR
METHYLENE IODIDE ON ROUGHENED NYLON SURFACES

| Smooth | | #120 Grit | | #180 Grit | | #240 Grit | |
|---|---|---|---|---|---|---|---|
| Velocity cm/sec | Angle degrees | Velocity cm/sec | Angle degrees | Velocity cm/sec | Angle degrees | Velocity cm/sec | Angle degrees |
| 0 | 41 | 0 | 51 | 0 | 54 | 0 | 52 |
| 0.00158 | 42 | 0.061 | 60 | 0.026 | 55 | 0.024 | 51 |
| 0.0035 | 46 | 0.111 | 64 | 0.046 | 56 | 0.057 | 56 |
| 0.011 | 45 | 0.172 | 65 | 0.073 | 40 | 0.093 | 61 |
| 0.022 | 46 | 0.312 | 66 | 0.111 | 42 | 0.149 | 61 |
| 0.12 | 46 | 0.318 | 66 | 0.343 | 49 | 0.179 | 46 |
| 0.133 | 50 | 0.452 | 64 | 0.490 | 53 | 0.245 | 44 |
| 0.140 | 48 | 0.932 | 67 | 0.932 | 58 | 0.330 | 47 |
| 0.180 | 49 | 1.118 | 67 | 1.677 | 64 | 0.429 | 48 |
| 0.322 | 52 | 1.863 | 74 | 2.795 | 70 | 0.686 | 60 |
| 0.341 | 51 | 2.236 | 72 | 3.540 | 75 | 0.932 | 61 |
| 0.40 | 49 | 2.795 | 75 | 4.472 | 81 | 1.770 | 68 |
| 1.1 | 60 | 3.354 | 76 | 5.031 | 83 | 2.795 | 69 |
| 1.4 | 62 | 3.727 | 77 | 5.590 | 90 | 3.727 | 77 |
| 1.86 | 64 | 5.776 | 89 | 6.521 | >90 | 4.845 | 82 |
| 2.8 | 67 | 6.894 | 85 | | | 5.776 | 83 |
| 3.1 | 69 | 9.317 | 89 | | | 6.801 | 86 |
| 4.2 | 71 | 9.689 | 90 | | | 7.640 | 90 |
| 4.4 | 72 | | | | | | |
| 6.2 | 79 | | | | | | |
| 10.2 | 90 | | | | | | |

TABLE VIII

DYNAMIC CONTACT ANGLE VELOCITY DATA FOR
HEXADECANE ON ROUGHENED STAINLESS STEEL SURFACES

| Smooth | | #120 Grit | | #180 Grit | | #240 Grit | |
|---|---|---|---|---|---|---|---|
| Velocity cm/sec | Angle degrees | Velocity cm/sec | Angle degrees | Velocity cm/sec | Angle degrees | Velocity cm/sec | Angle degrees |
| 0 | 0 | 0 | 0 | 0 | 0 | 0 | 0 |
| 0.82 | 35 | 0.059 | 16 | 0.045 | 11 | 0.027 | 6 |
| 1.97 | 45 | 0.080 | 21 | 0.062 | 14 | 0.029 | 9 |
| 3.02 | 54 | 0.118 | 25 | 0.066 | 16 | 0.045 | 7 |
| 3.85 | 59 | 0.156 | 30 | 0.088 | 21 | 0.049 | 7 |
| 4.77 | 64 | 0.209 | 41 | 0.114 | 24 | 0.084 | 13 |
| 6.40 | 71 | 0.286 | 38 | 0.156 | 29 | 0.098 | 10 |
| 6.48 | 67 | 0.336 | 36 | 0.163 | 26 | 0.172 | 14 |
| 7.72 | 74 | 1.118 | 42 | 0.209 | 32 | 0.226 | 16 |
| 8.60 | 76 | 1.677 | 47 | 0.260 | 34 | 0.238 | 17 |
| 10.45 | 76 | 2.888 | 56 | 0.429 | 36 | 0.838 | 26 |
| 11.70 | 77 | 3.727 | 62 | 0.931 | 41 | 1.770 | 37 |
| 12.90 | 78 | 4.658 | 67 | 1.770 | 48 | 3.261 | 54 |
| 13.60 | 79 | 5.590 | 74 | 2.981 | 58 | 3.727 | 61 |
| 15.20 | 80 | 6.894 | 76 | 3.727 | 62 | 6.522 | 71 |
| | | 7.453 | 77 | 4.752 | 68 | 7.453 | 76 |
| | | 8.571 | 80 | 5.590 | 72 | 7.453 | 77 |
| | | 9.317 | 82 | 6.708 | 76 | 7.826 | 79 |
| | | 10.150 | 86 | 7.268 | 82 | | |
| | | 12.180 | 90 | 8.571 | 81 | | |
| | | | | 9.503 | 84 | | |
| | | | | 10.150 | 85 | | |
| | | | | 15.225 | >90 | | |

TABLE IX

DYNAMIC CONTACT ANGLE-VELOCITY DATA FOR
ABSOLUTE ALCOHOL ON ROUGHENED STAINLESS STEEL SURFACES

| Smooth | | #120 Grit | | #180 Grit | | #240 Grit | |
|---|---|---|---|---|---|---|---|
| Velocity cm/sec | Angle degrees | Velocity cm/sec | Angle degrees | Velocity cm/sec | Angle degrees | Velocity cm/sec | Angle degrees |
| 0 | 0 | 0 | 0 | 0 | 0 | 0 | 0 |
| 3.75 | 42 | 0.016 | 45 | 0.053 | 44 | 0.024 | 45 |
| 5.80 | 52 | 0.036 | 46 | 0.069 | 43 | 0.062 | 44 |
| 8.02 | 57 | 0.043 | 47 | 0.049 | 44 | 0.086 | 43 |
| 8.99 | 62 | 0.055 | 48 | 0.028 | 44 | 0.13 | 44 |
| 12.7 | 64 | 0.067 | 49 | 0.076 | 45 | 0.182 | 43 |
| 13.25 | 64 | 0.114 | 51 | 0.098 | 44 | 0.25 | 44 |
| 19.1 | 65 | 0.153 | 53 | 0.122 | 45 | 0.95 | 47 |
| 19.1 | 66 | 0.350 | 51 | 0.277 | 47 | 2.05 | 49 |
| 28.7 | 73 | 0.950 | 53 | 0.95 | 56 | 2.8 | 51 |
| 32.3 | 74 | 1.88 | 54 | 1.675 | 58 | 3.7 | 53 |
| 32.3 | 75 | 3.20 | 59 | 2.60 | 59 | 4.65 | 54 |
| 36.8 | 76 | 4.65 | 60 | 3.35 | 59 | 5.90 | 56 |
| 39.7 | 80 | 5.55 | 68 | 5.00 | 60 | 6.85 | 58 |
| | | 8.50 | 71 | 5.75 | 62 | 7.75 | 58 |
| | | 10.20 | 70 | 6.65 | 62 | | |
| | | 15.30 | 72 | 7.57 | 64 | | |
| | | 30.20 | 80 | 9.25 | 68 | | |

TABLE X

DYNAMIC CONTACT ANGLE-VELOCITY DATA FOR
HEXANE ON ROUGHENED STAINLESS STEEL SURFACES

| Smooth | | #120 Grit | | #180 Grit | | #240 Grit | |
|---|---|---|---|---|---|---|---|
| Velocity cm/sec | Angle degrees | Velocity cm/sec | Angle degrees | Velocity cm/sec | Angle degrees | Velocity cm/sec | Angle degrees |
| 0 | 0 | 0 | 0 | 0 | 0 | 0 | 0 |
| 3.86 | 47 | 0.34 | 0 | 0.06 | 0 | 0.25 | 0 |
| 6.48 | 52 | 0.48 | 0 | 0.07 | 0 | 0.40 | 0 |
| 11.12 | 55 | 0.52 | 0 | 0.14 | 0 | 1.15 | 0 |
| 14.13 | 59 | 0.72 | 38 | 0.19 | 0 | 1.87 | 45 |
| 17.06 | 61 | 0.82 | 38 | 0.23 | 0 | 2.80 | 48 |
| 21.54 | 62 | 0.95 | 41 | 0.29 | 0 | 3.90 | 48 |
| 25.86 | 63 | 1.86 | 42 | 0.43 | 0 | 5.00 | 50 |
| 32.35 | 66 | 2.80 | 42 | 0.49 | 0 | 5.50 | 50 |
| 34.51 | 67 | 3.70 | 44 | 0.57 | 43 | 7.20 | 53 |
| 43.08 | 67 | 4.65 | 46 | 1.85 | 44 | 10.20 | 56 |
| 57.44 | 67 | 9.55 | 50 | 2.80 | 45 | 14.2 | 58 |
| 64.69 | 67 | 10.2 | 53 | 3.72 | 47 | 19.3 | 62 |
| | | 15.3 | 58 | 8.20 | 51 | 26.3 | 62 |
| | | 20.3 | 61 | 10.2 | 55 | | |
| | | 30.3 | 64 | 15.3 | 53 | | |
| | | | | 21.3 | 59 | | |
| | | | | 25.3 | 61 | | |

TABLE XI

DYNAMIC CONTACT ANGLE-VELOCITY DATA FOR HEXANE AND ROUGHENED NYLON SURFACES

| Smooth | | #120 Grit | | #180 Grit | | #240 Grit | |
|---|---|---|---|---|---|---|---|
| Velocity cm/sec | Angle degrees | Velocity cm/sec | Angle degrees | Velocity cm/sec | Angle degrees | Velocity cm/sec | Angle degrees |
| 0 | 0 | 0 | 0 | 0 | 0 | 0 | 0 |
| 3.97 | 44 | 0.06 | 0 | 0.08 | 0 | 0.29 | 0 |
| 7.12 | 49 | 0.09 | 0 | 0.10 | 0 | 0.54 | 0 |
| 11.55 | 51 | 0.12 | 0 | 0.18 | 0 | 0.90 | 0 |
| 18.40 | 53 | 0.45 | 0 | 0.24 | 0 | 1.37 | 0 |
| 21.40 | 53 | 0.24 | 0 | 0.36 | 0 | 1.50 | 0 |
| 22.70 | 56 | 0.34 | 0 | 0.40 | 0 | 2.05 | 40 |
| 29.10 | 56 | 0.42 | 0 | 0.75 | 0 | 2.80 | 40 |
| 31.40 | 56 | 0.54 | 0 | 1.87 | 0 | 4.10 | 45 |
| 34.30 | 60 | 1.87 | 0 | 3.0 | 44 | 4.82 | 47 |
| 36.80 | 60 | 2.80 | 43 | 3.9 | 46 | 5.92 | 50 |
| 37.20 | 56 | 3.70 | 45 | 4.65 | 44 | 10.20 | 49 |
| 48.00 | 57 | 4.82 | 46 | 5.55 | 48 | 7.20 | 50 |
| 51.50 | 65 | 6.50 | 48 | 7.75 | 49 | 15.20 | 59 |
| 64.90 | 70 | 7.57 | 47 | 9.60 | 52 | 20.2 | 59 |
| | | 9.55 | 48 | 10.3 | 53 | 25.3 | 60 |
| | | 10.20 | 49 | 15.3 | 54 | 32.3 | 61 |
| | | 15.30 | 51 | 20.3 | 54 | 36.2 | 64 |
| | | 21.30 | 53 | 26.3 | 56 | 41.3 | 67 |
| | | 25.30 | 55 | 35.2 | 59 | 45.3 | 70 |
| | | 30.20 | 58 | 42.4 | 60 | | |
| | | 40.20 | 60 | | | | |
| | | 50.2 | 63 | | | | |

TABLE XII

DYNAMIC CONTACT ANGLE-VELOCITY DATA FOR
HEXANE ON ROUGHENED POLY(METHYL METHACRYLATE) SURFACES

| Smooth | | #120 Grit | | #180 Grit | | #240 Grit | |
|---|---|---|---|---|---|---|---|
| Velocity cm/sec | Angle degrees | Velocity cm/sec | Angle degrees | Velocity cm/sec | Angle degrees | Velocity cm/sec | Angle degrees |
| 0 | 0 | 0 | 0 | 0 | 0 | 0 | 0 |
| 2.65 | 44 | 0.214 | 40 | 0.240 | 37 | 0.143 | 32 |
| 8.68 | 50 | 0.268 | 41 | 0.572 | 37 | 0.572 | 36 |
| 12.1 | 52 | 0.440 | 41 | 1.372 | 42 | 0.558 | 36 |
| 17.7 | 56 | 0.858 | 41 | 1.87 | 45 | 2.05 | 41 |
| 20.4 | 56 | 1.107 | 45 | 3.00 | 43 | 2.79 | 41 |
| 30.3 | 58 | 1.806 | 46 | 3.7 | 46 | 3.91 | 44 |
| 32.3 | 61 | 3.0 | 47 | 4.82 | 43 | 4.65 | 42 |
| 35.2 | 61 | 3.7 | 47 | 5.75 | 47 | 5.58 | 45 |
| 39.7 | 61 | 4.65 | 51 | 8.02 | 45 | 5.03 | 43 |
| 47.0 | 63 | 5.95 | 51 | 10.6 | 46 | 8.05 | 48 |
| 57.0 | 67 | 8.2 | 52 | 15.1 | 48 | 10.06 | 47 |
| 62.9 | 67 | 10.2 | 54 | 20.13 | 52 | 13.09 | 50 |
| 70.9 | 67 | 15.3 | 54 | 26.2 | 55 | 15.1 | 54 |
| | | 20.3 | 56 | 35.3 | 58 | 18.2 | 56 |
| | | 25.3 | 57 | 41.3 | 59 | 20.13 | 55 |
| | | 33.5 | 61 | 45.3 | 63 | 25.16 | 56 |
| | | 36.2 | 62 | 50.3 | 64 | 31.2 | 62 |
| | | | | | | 37.2 | 63 |
| | | | | | | 41.3 | 66 |
| | | | | | | 48.3 | 70 |

TABLE XIII

ROUGHENED STAINLESS STEEL SYSTEMS

| | | Smooth | #120 | #180 | #240 |
|---|---|---|---|---|---|
| Hexadecane | Slope slow side | --- | .17 | .14 | .05 |
| | Slope fast side | .53 | .80 | .84 | .84 |
| | Vc cm/sec | --- | 1.7 | 1.6 | 1.3 |
| | Lowest V measured cm/sec | .82 | .06 | .04 | .02 |
| Alcohol | Slope slow side | --- | .05 | .04 | .02 |
| | Slope fast side | .54 | .27 | .19 | .22 |
| | Vc cm/sec | --- | 1.0 | .22 | 1.2 |
| | Lowest V measured cm/sec | 3.8 | .02 | .03 | .03 |
| Hexane | Slope slow side | --- | 0[a] | 0[a] | 0[a] |
| | Slope fast side | .30 | .23 | .18 | .21 |
| | Vc cm/sec | --- | .7 | .5 | 1.2 |
| | Lowest V measured cm/sec | 3.8 | .35 | .06 | .25 |

a. This is an Elliott-Riddiford type system (refs. 10, 11).

TABLE XIV

ROUGHENED NYLON SYSTEMS

| | | Smooth | #120 | #180 | #240 |
|---|---|---|---|---|---|
| Alpha Bronopaphthalene | Slope slow side | .08 | .04 | .15 | .12 |
| | Slope fast side | .50 | .45 | .47 | .61 |
| | Vc cm/sec | .25 | .13 | .15 | .70 |
| | Lowest V measured | .02 | .04 | .04 | .03 |
| Hexane | Slope slow side | --- | 0[a] | 0[a] | 0[a] |
| | Slope fast side | .22 | .22 | .28 | .30 |
| | Vc cm/sec | --- | 2.0 | 2.5 | 1.5 |
| | Lowest V measured | 4.0 | .06 | .08 | .30 |
| Water | Slope slow side | .04 | (b) | (b) | (b) |
| | Slope fast side | .12 | (b) | (b) | (b) |
| | Vc cm/sec | .002 | (b) | (b) | (b) |
| | Lowest V measured | .0004 | (b) | (b) | (b) |
| Methylene iodide | Slope slow side | .05 | .08 | .04 | .07 |
| | Slope fast side | .52 | .44 | .6 | .55 |
| | Vc cm/sec | .80 | 1.0 | 1.1 | 1.1 |
| | Lowest V measured | .002 | .06 | .02 | .02 |

a. This is an Elliott-Riddiford type system (refs. 10, 11).
b. Measurements cover less than one decade of velocity.

TABLE XV

ROUGHENED PMMA-HEXANE SYSTEM

| | | Smooth | #120 | #180 | #240 |
|---|---|---|---|---|---|
| Hexane | Slope slow side | --- | .06 | .07 | .08 |
| | Slope fast side | .25 | .20 | .40 | .44 |
| | Vc cm/sec | --- | 3.8 | 10.0 | 8.0 |
| | Lowest V measured | 2.7 | .20 | .24 | .15 |

TABLE XVI

ROUGHENED TEFLON SYSTEMS

| | | Smooth | #120 | #180 | #240 |
|---|---|---|---|---|---|
| Dioctyl sebacate | Slope slow side | .05 | .13 | .08 | .16 |
| | Slope fast side | .22 | .35 | .30 | .29 |
| | Vc cm/sec | .08 | .10 | .05 | .08 |
| | Lowest V measured | .02 | .01 | .003 | .01 |
| Octane | Slope slow side | .17 | .07 | .05 | .05 |
| | Slope fast side | .75 | .55 | .40 | .44 |
| | Vc cm/sec | 25.0 | 6.0 | 2.5 | 3.5 |
| | Lowest V measured | .4 | .05 | .06 | .09 |

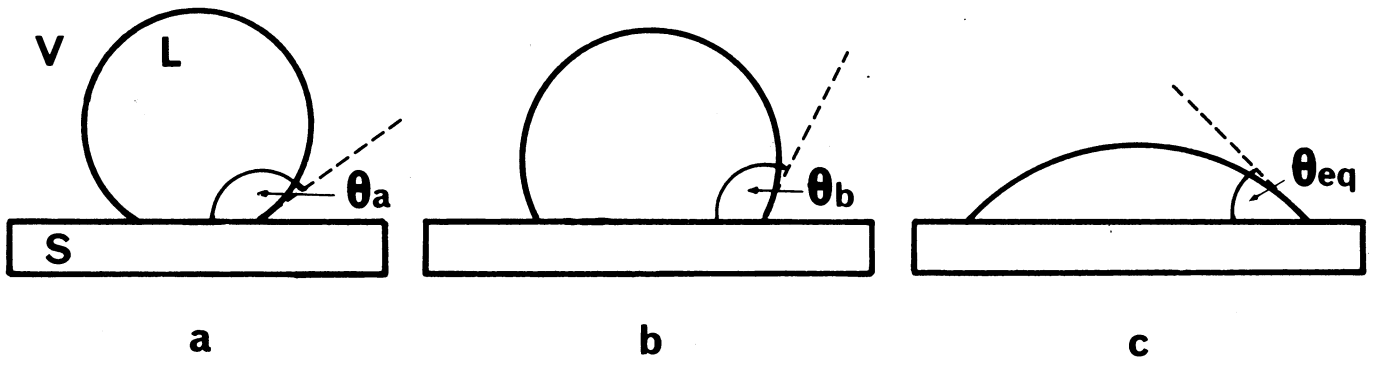


Figure 1. Stages in self-spreading of a drop.

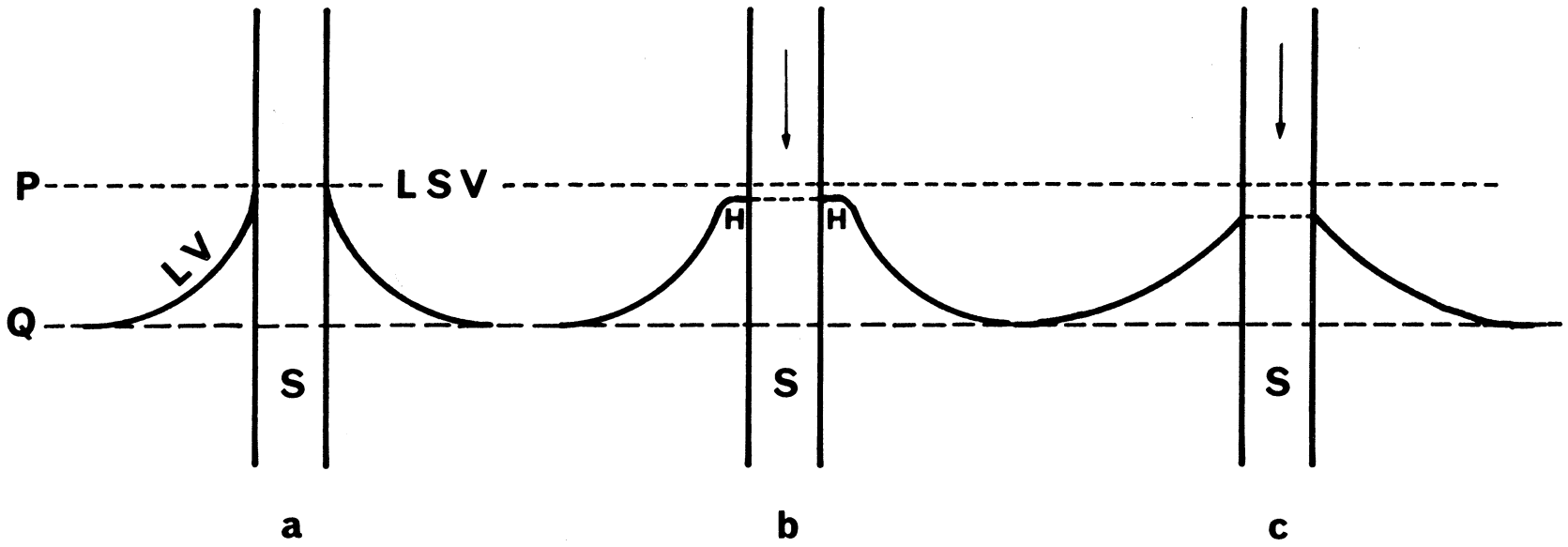


Figure 2. Establishment of a dynamic contact angle. Forced spreading. Arrow shows direction of motion of solid S. Dotted line P is equilibrium level of LSV boundary. Dashed line Q is liquid level baseline.

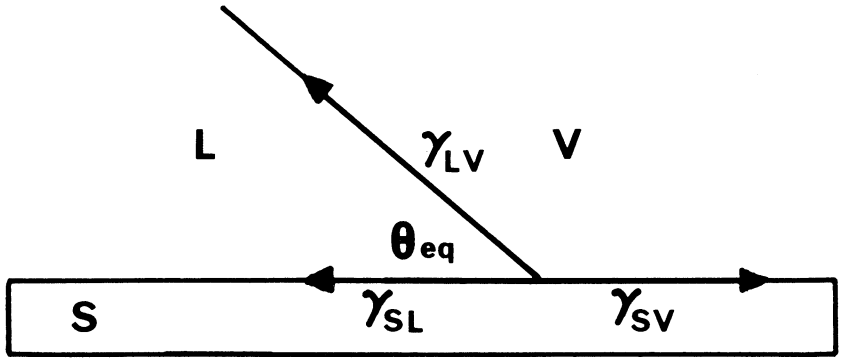


Figure 3. Balance of forces at $\theta = \theta_{eq}$ (Young's equation).

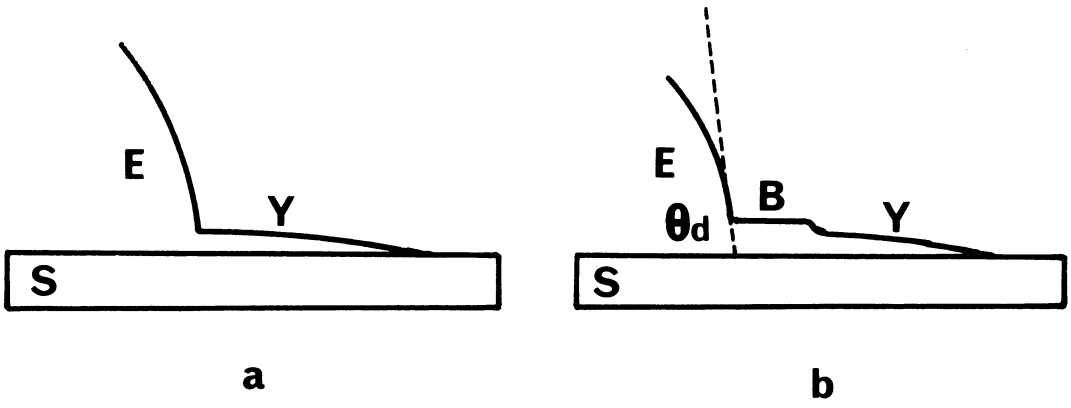


Figure 4. Primary (Y) and secondary (B) layers in self-spreading.

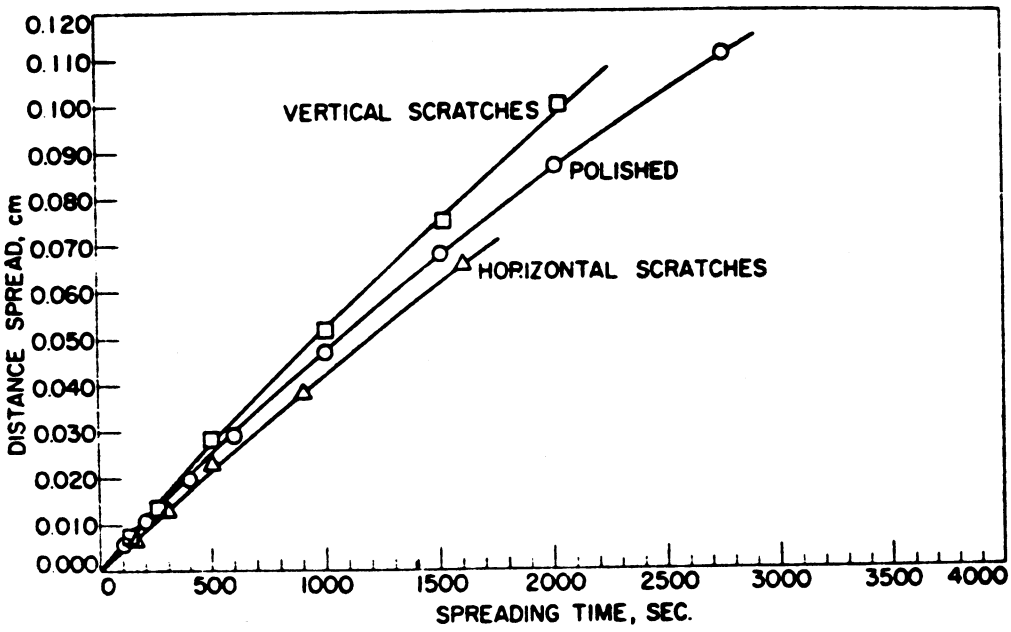


Figure 5. Effect of directional scratches on distance versus time for 10% pristane in distilled squalene on vertical steel plates. (From reference 5).

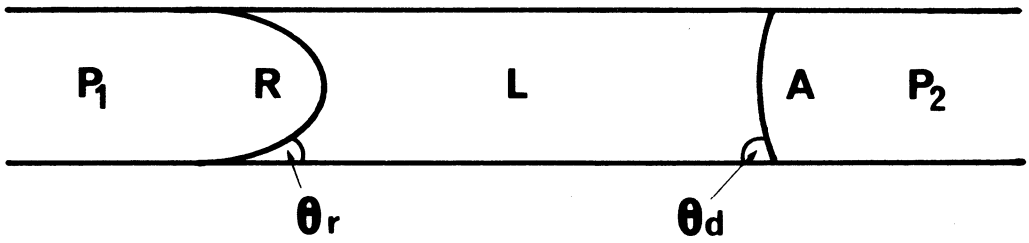


Figure 6. Rose-Heins system. Liquid moves from R toward A under pressure difference $P_1$-$P_2$.

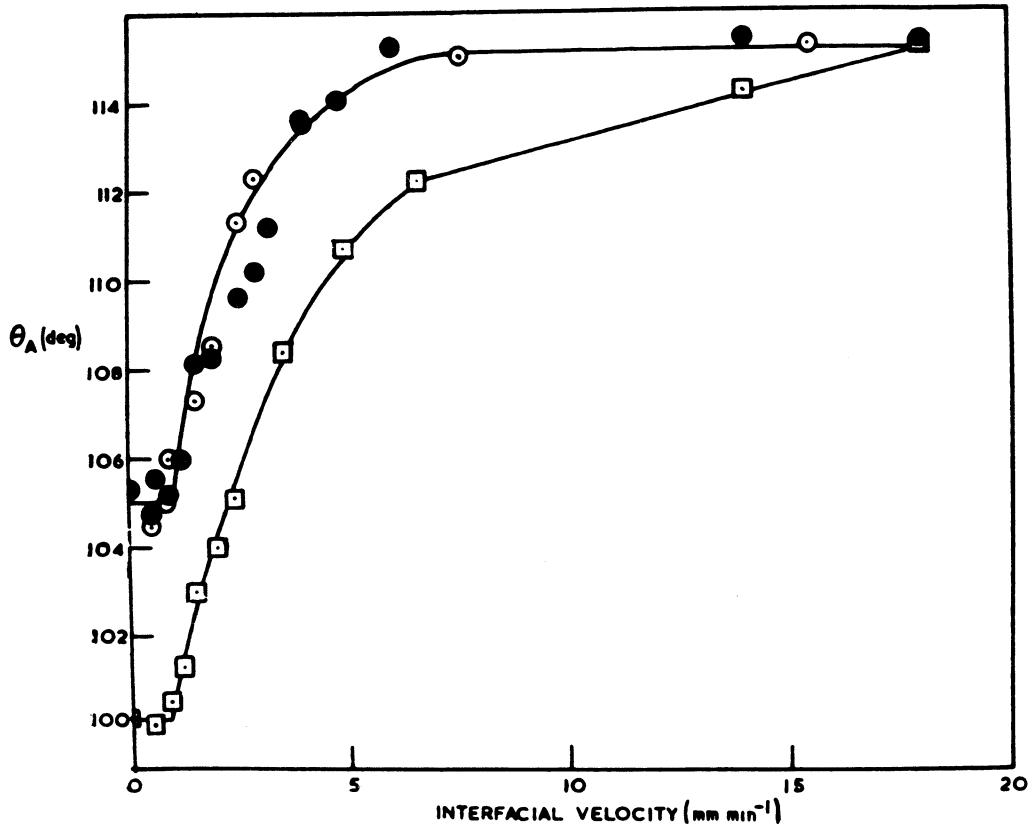


Figure 7. Advancing contact angles as a function of the velocity of an air/water interface moving over siliconed glass at 22°C, (-●-), siliconed glass at 42°C, (-⊙-), and polyethylene at 22°C, (-⊡-). (From reference 11).

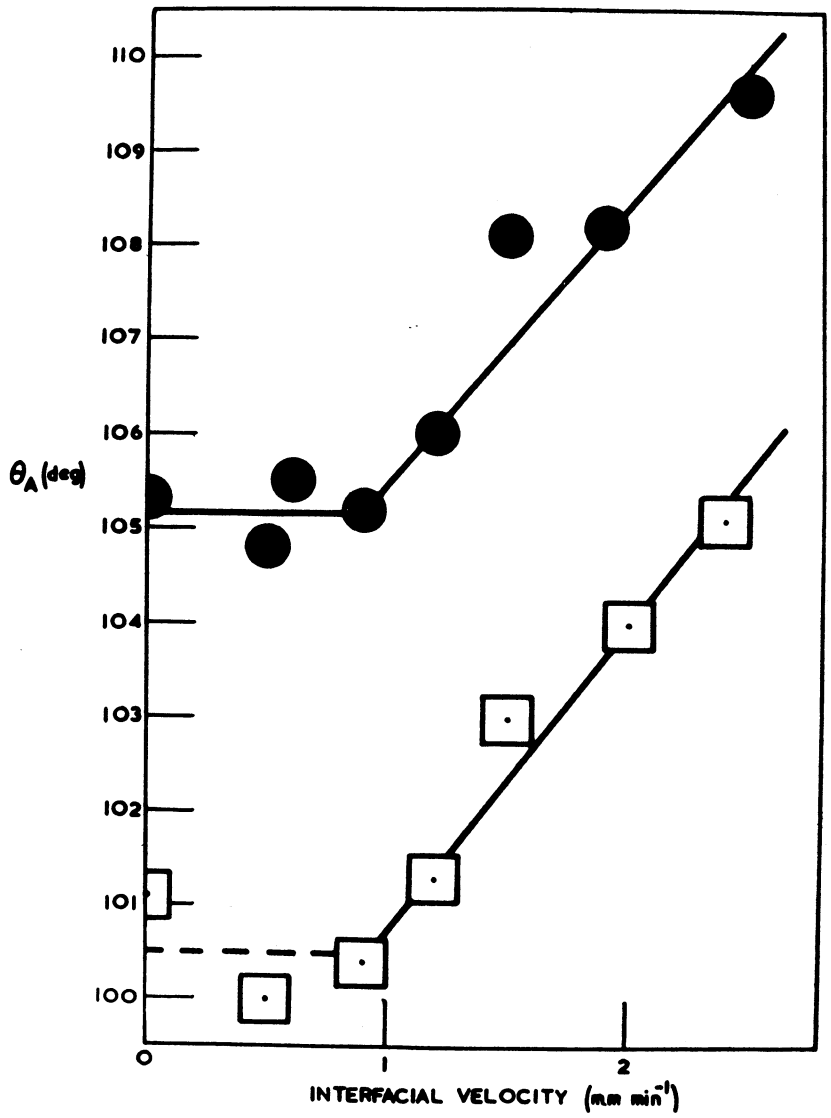


Figure 8. An expansion of part of Figure 7 showing the low velocity regions at 22°C. for a siliconed glass surface (-●-) and polyethylene (-⊡-). (From reference 11).

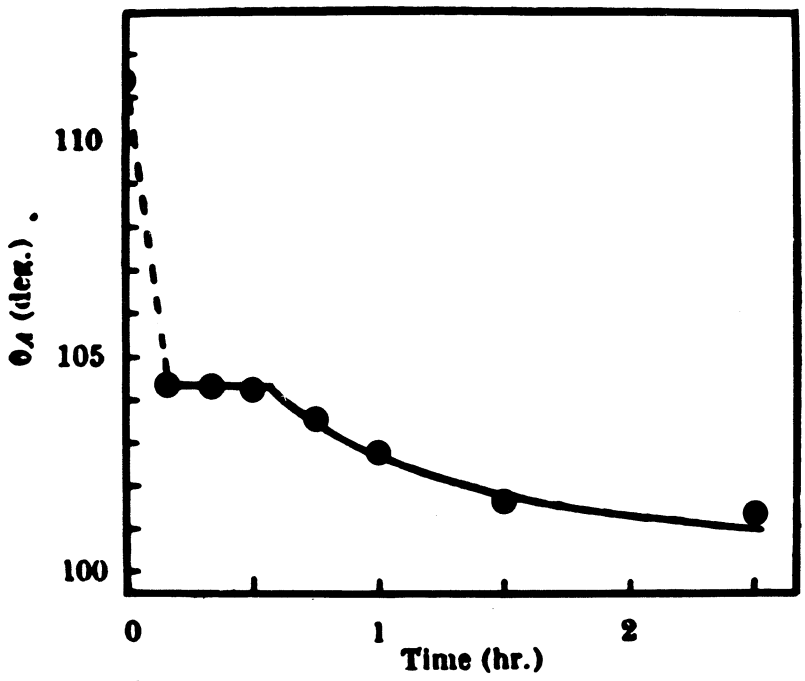


Figure 9. Relaxation of $\theta_d$ (designated $\theta_A$ in the diagram) after halting the interface from a velocity of 3 mm/min. (From reference 10).

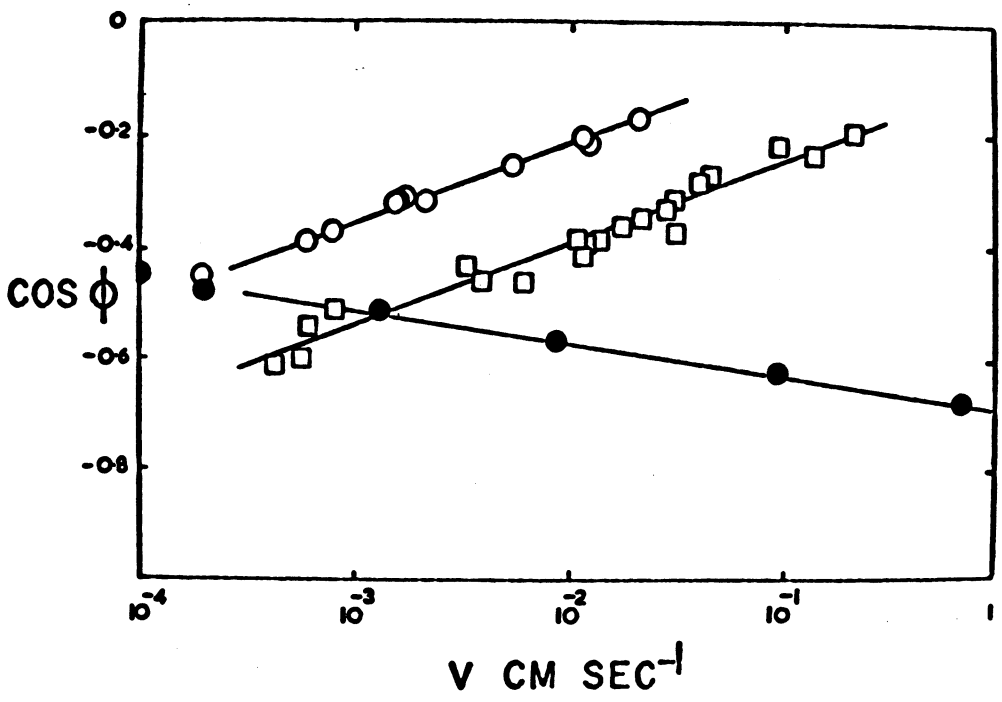


Figure 10. Advancing and receding dynamic contact angles. Benzene-water-siliconed glass. ○ and □ benzene advancing toward water in two slightly different tubes. ● water advancing toward benzene. (From reference 15).

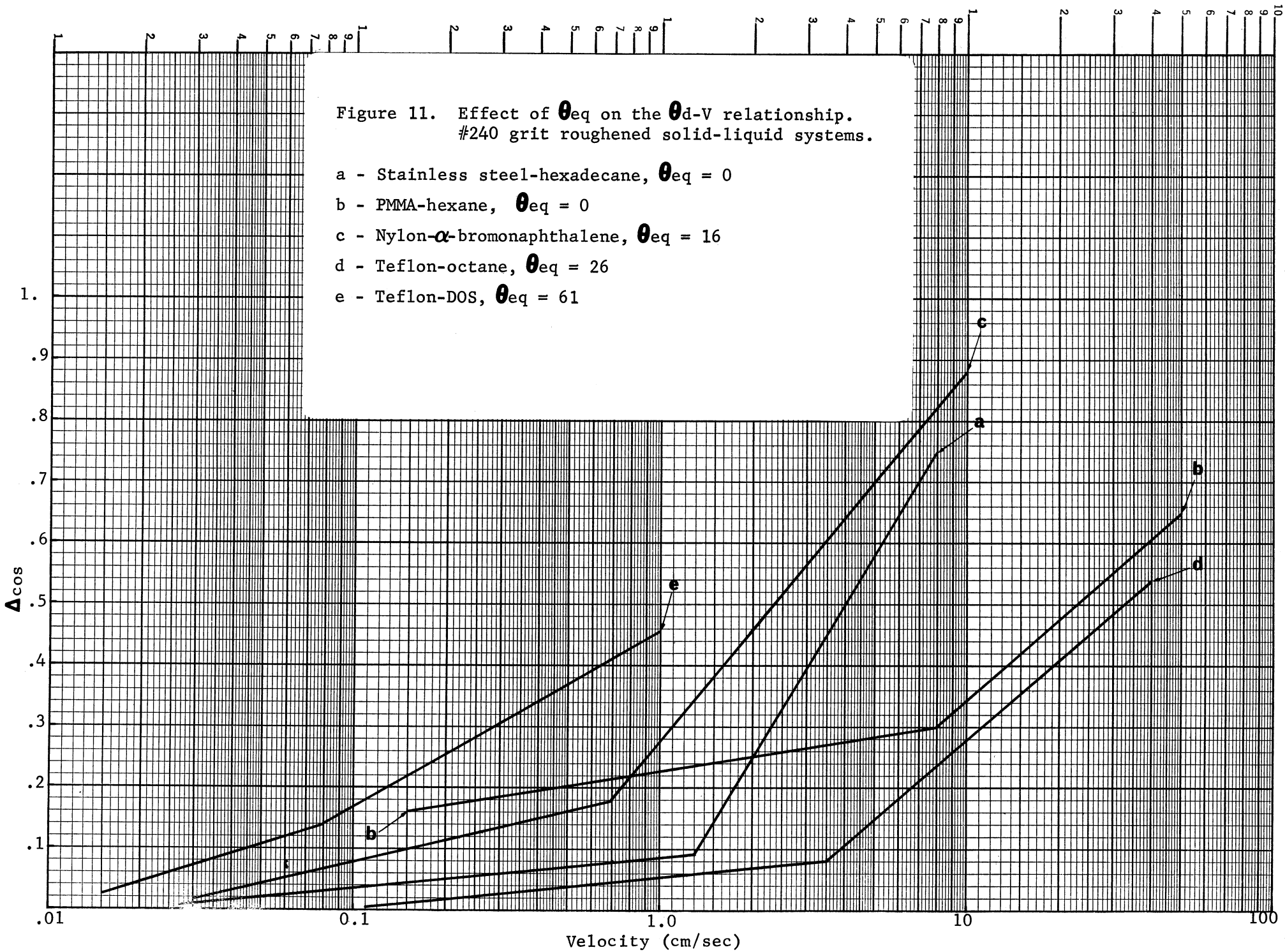
Figure 11. Effect of θeq on the θd-V relationship.
#240 grit roughened solid-liquid systems.
a - Stainless steel-hexadecane, θeq = 0
b - PMMA-hexane, θeq = 0
c - Nylon-α-bromonaphthalene, θeq = 16
d - Teflon-octane, θeq = 26
e - Teflon-DOS, θeq = 61
Δcos
1.
.9
.8
.7
.6
.5
.4
.3
.2
.1
.01
0.1
1.0
10
100
Velocity (cm/sec)
a
b
c
d
e

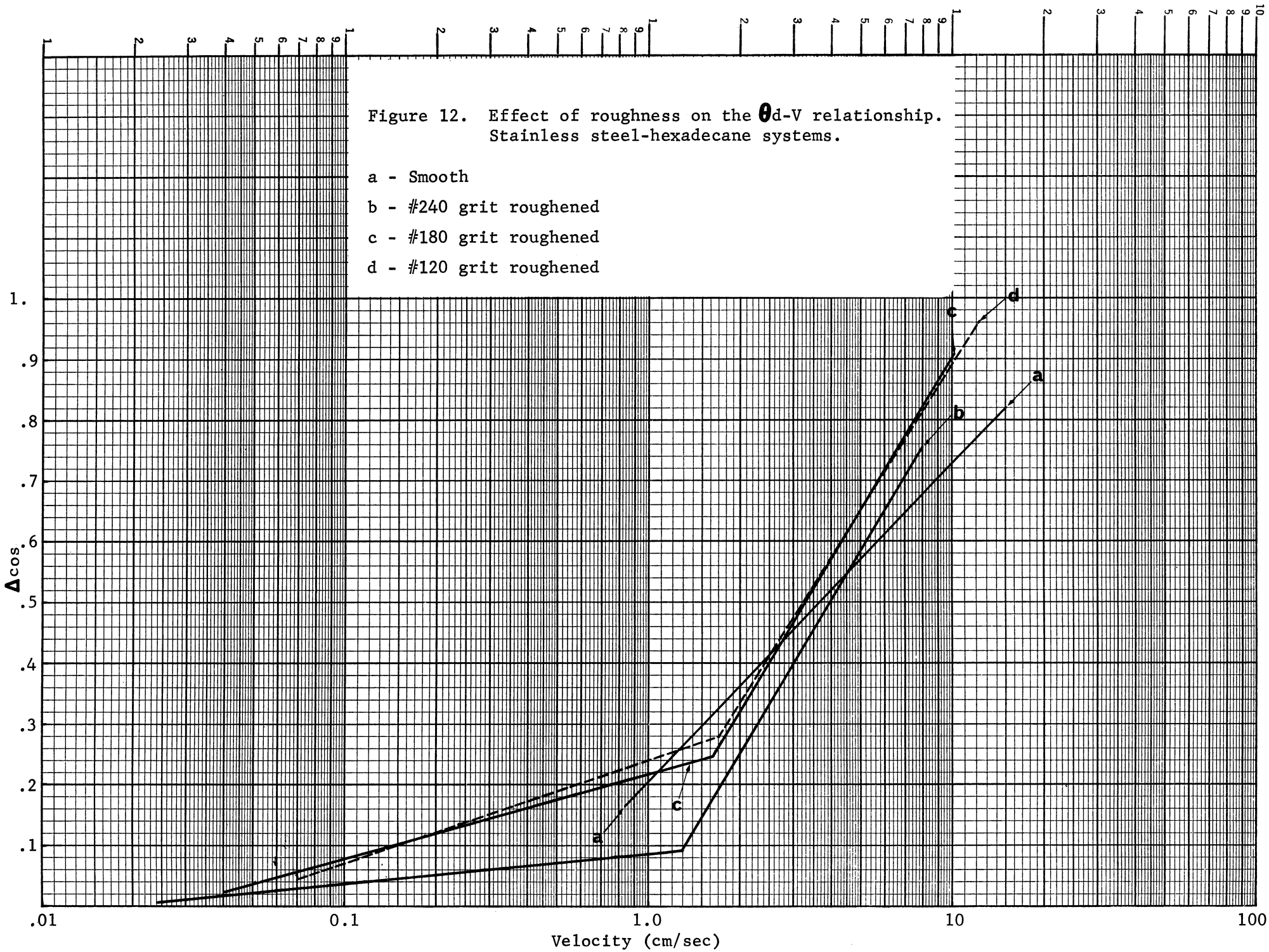
Figure 12. Effect of roughness on the θd-V relationship. Stainless steel-hexadecane systems.
a - Smooth
b - #240 grit roughened
c - #180 grit roughened
d - #120 grit roughened
Δcos
1.
.9
.8
.7
.6
.5
.4
.3
.2
.1
.01
0.1
1.0
10
100
Velocity (cm/sec)
a
b
c
d

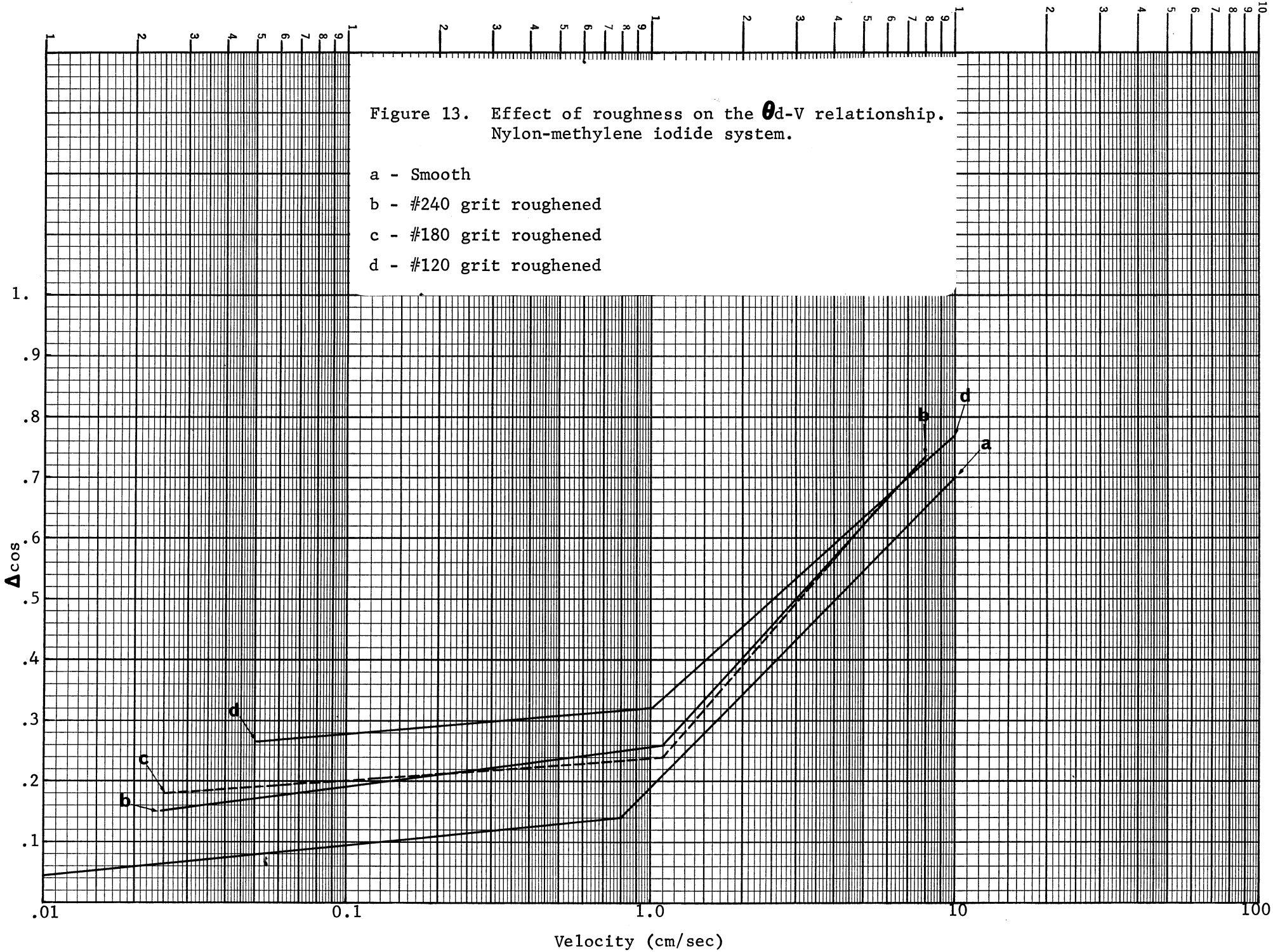
Figure 13. Effect of roughness on the θd-V relationship. Nylon-methylene iodide system.
a - Smooth
b - #240 grit roughened
c - #180 grit roughened
d - #120 grit roughened
Δcos
1.
.9
.8
.7
.6
.5
.4
.3
.2
.1
.01
0.1
1.0
10
100
Velocity (cm/sec)
a
b
c
d

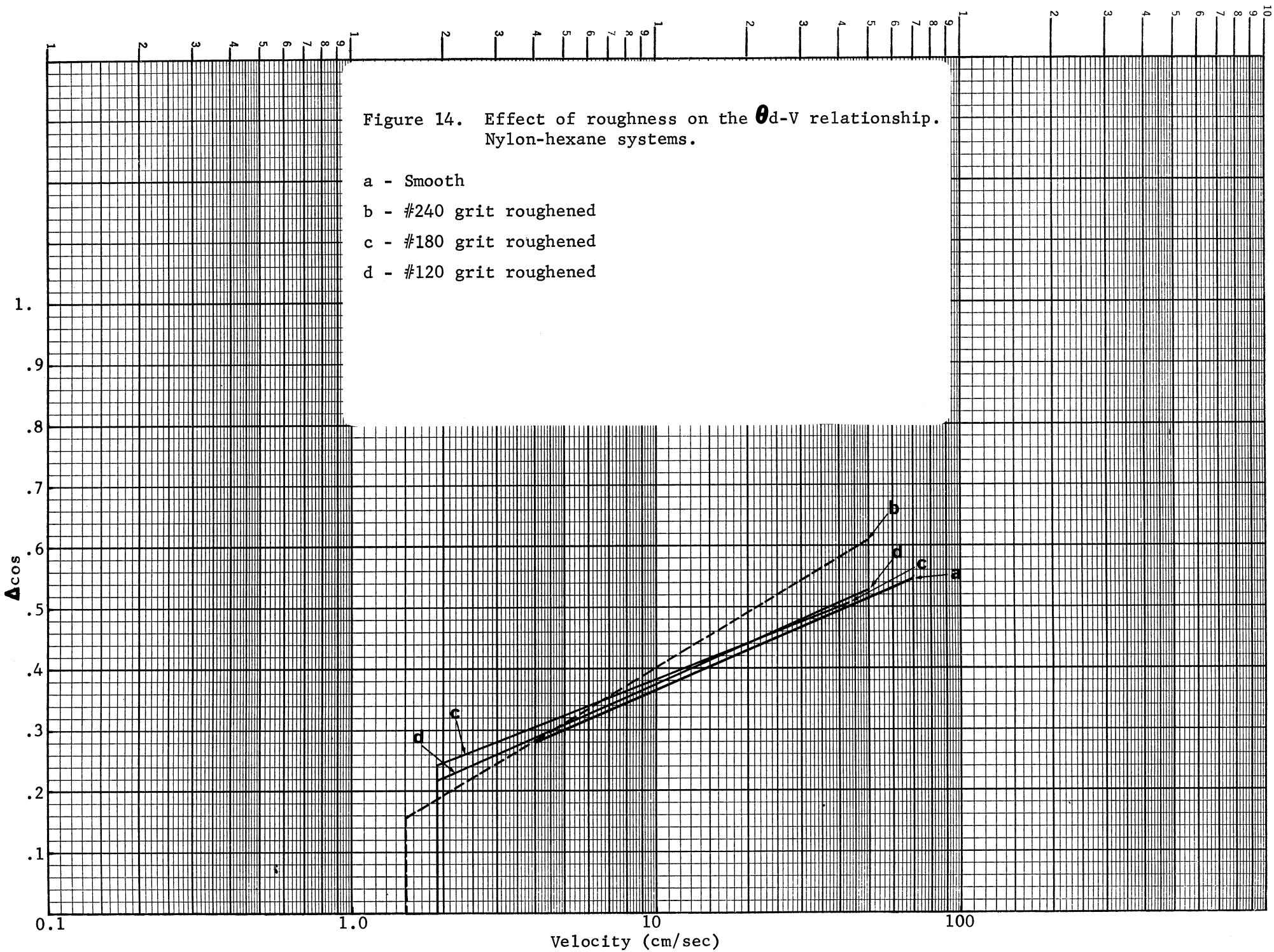
Figure 14. Effect of roughness on the θd-V relationship. Nylon-hexane systems.
a - Smooth
b - #240 grit roughened
c - #180 grit roughened
d - #120 grit roughened
1.
.9
.8
.7
.6
.5
.4
.3
.2
.1
Δcos
0.1
1.0
10
100
Velocity (cm/sec)
a
b
c
d

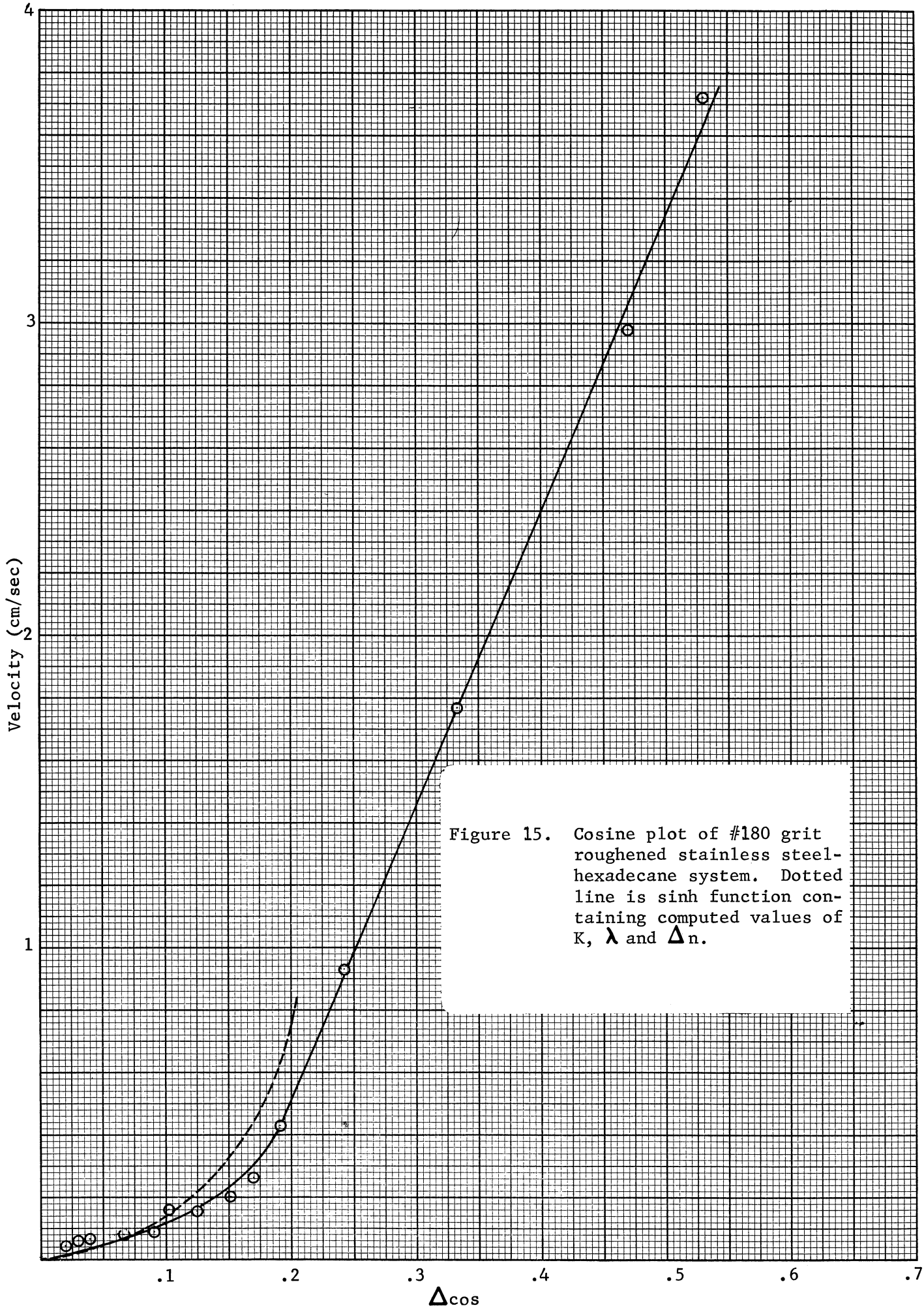


Figure 15. Cosine plot of #180 grit roughened stainless steel-hexadecane system. Dotted line is sinh function containing computed values of K, $\lambda$ and $\Delta$n.

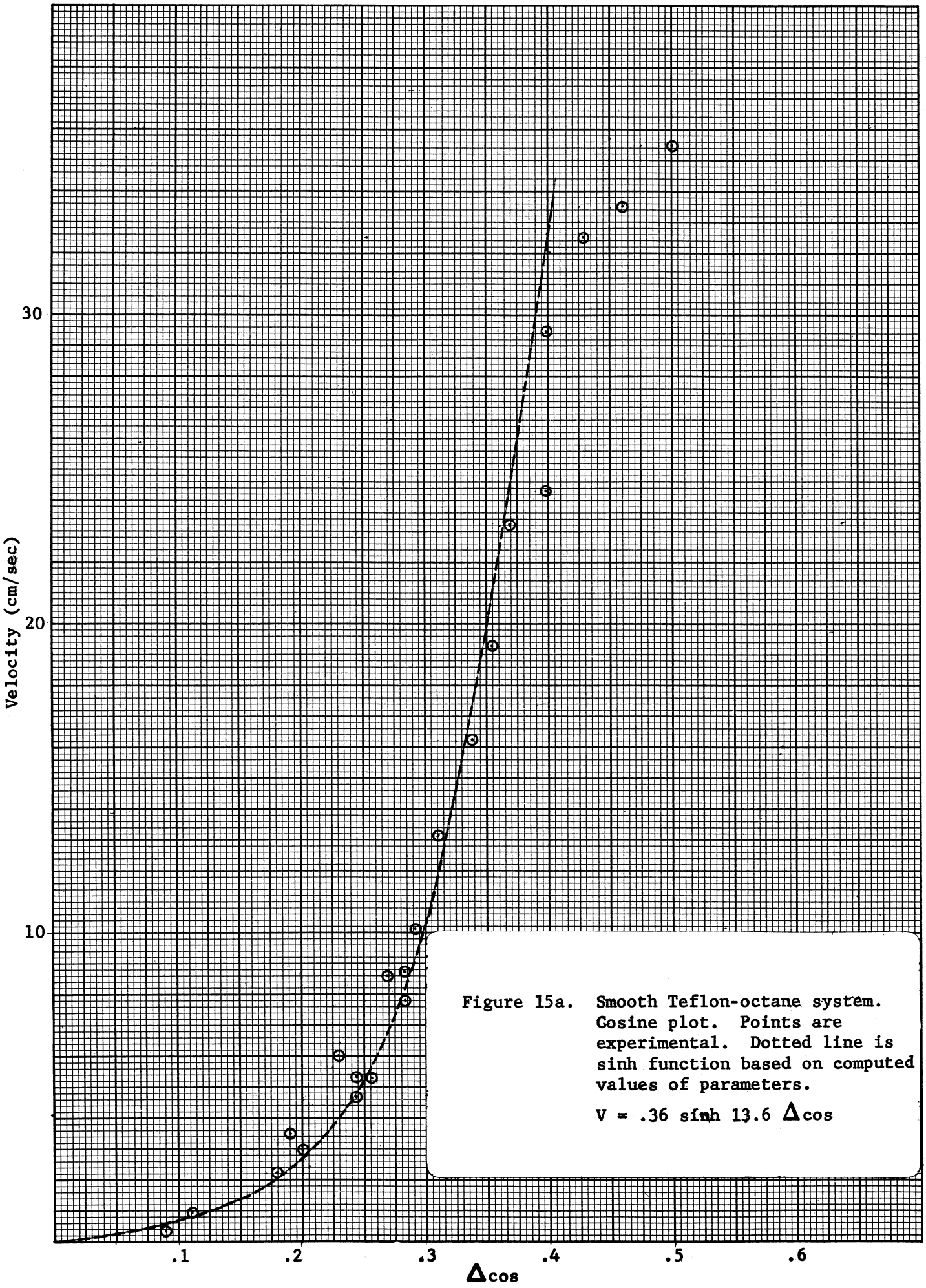


Figure 15a. Smooth Teflon-octane system. Cosine plot. Points are experimental. Dotted line is sinh function based on computed values of parameters.

$V = .36 \sinh 13.6 \Delta\cos$

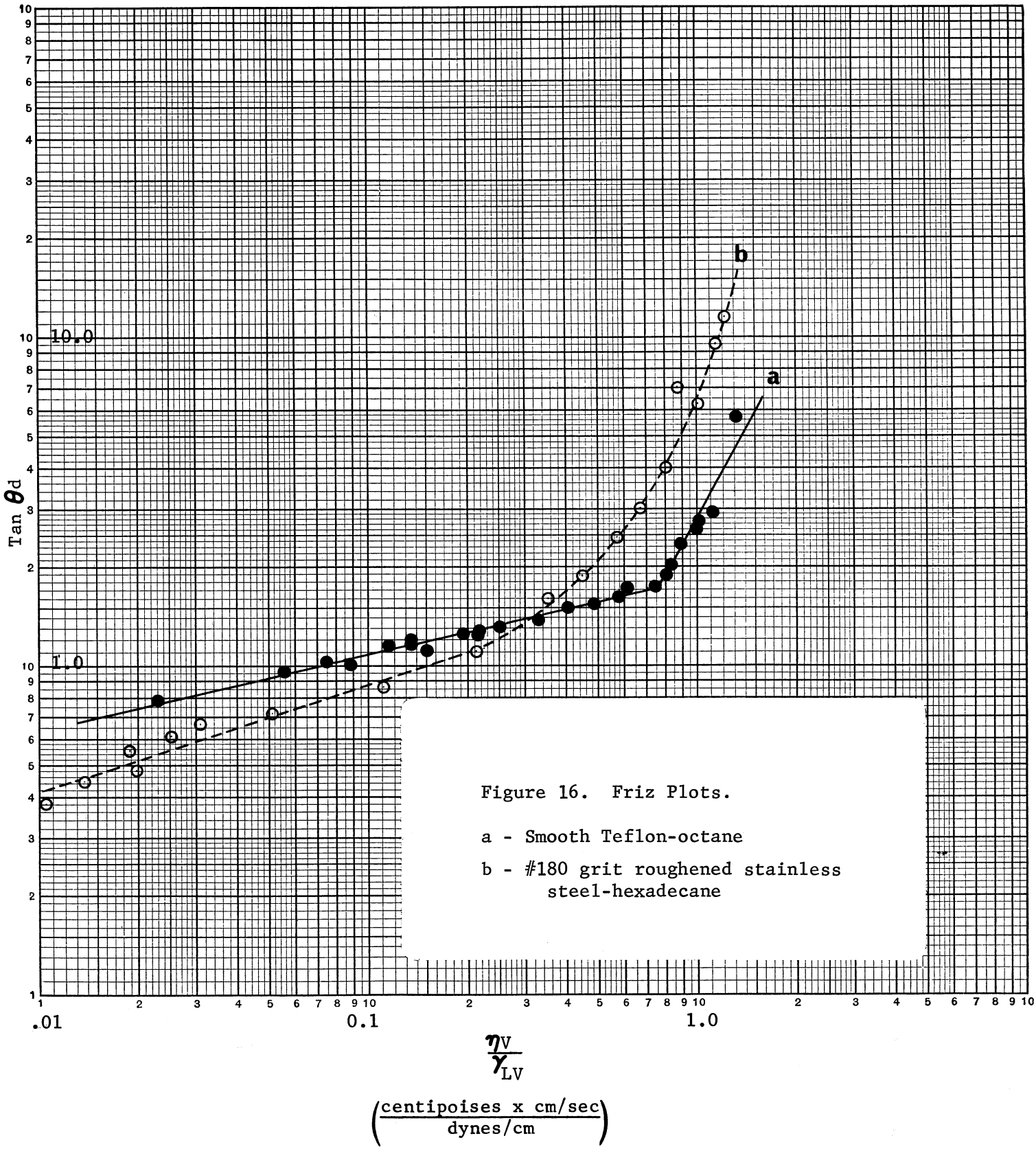


Figure 16. Friz Plots.

a - Smooth Teflon-octane

b - #180 grit roughened stainless steel-hexadecane

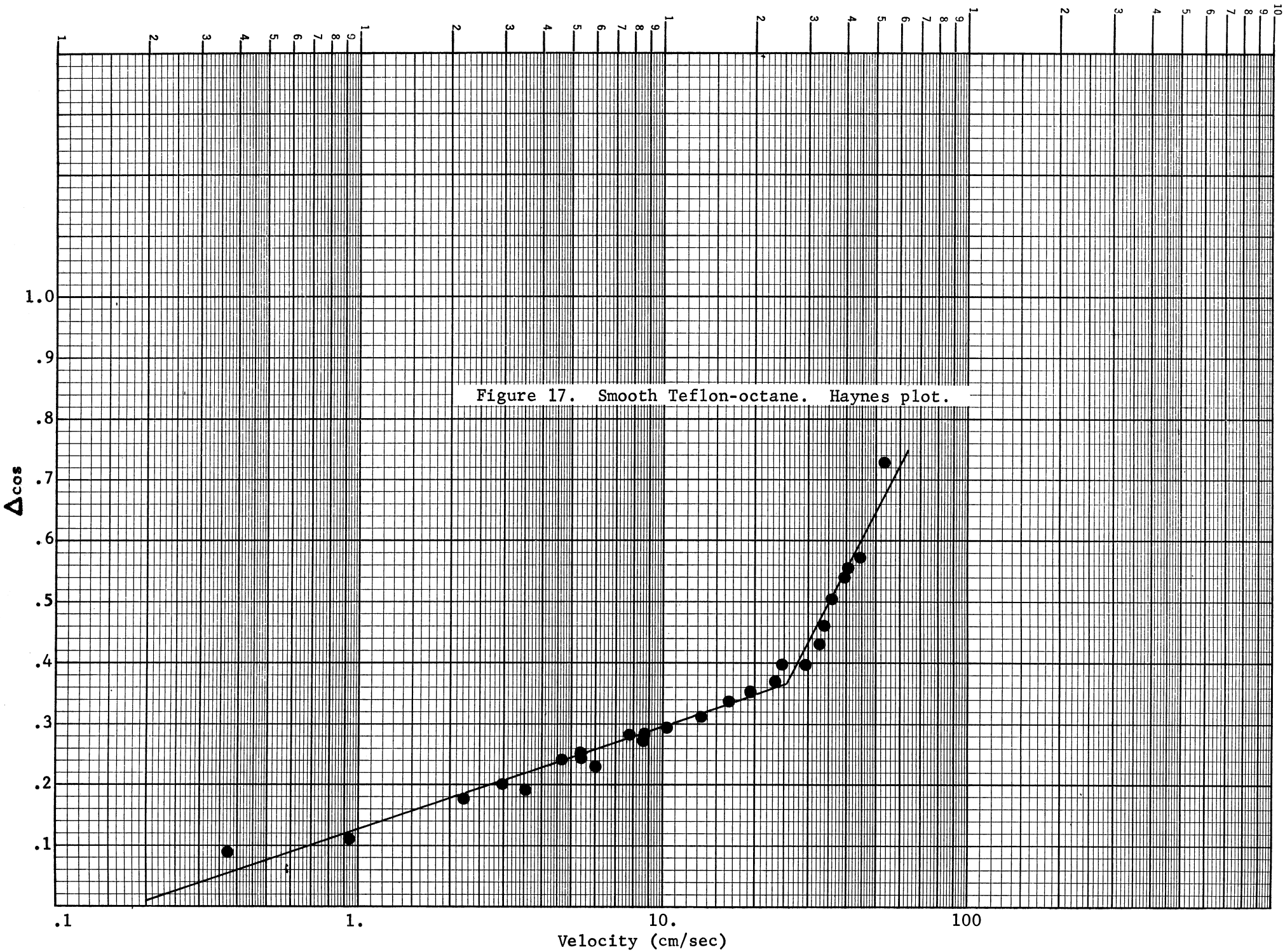


Figure 17. Smooth Teflon-octane. Haynes plot.

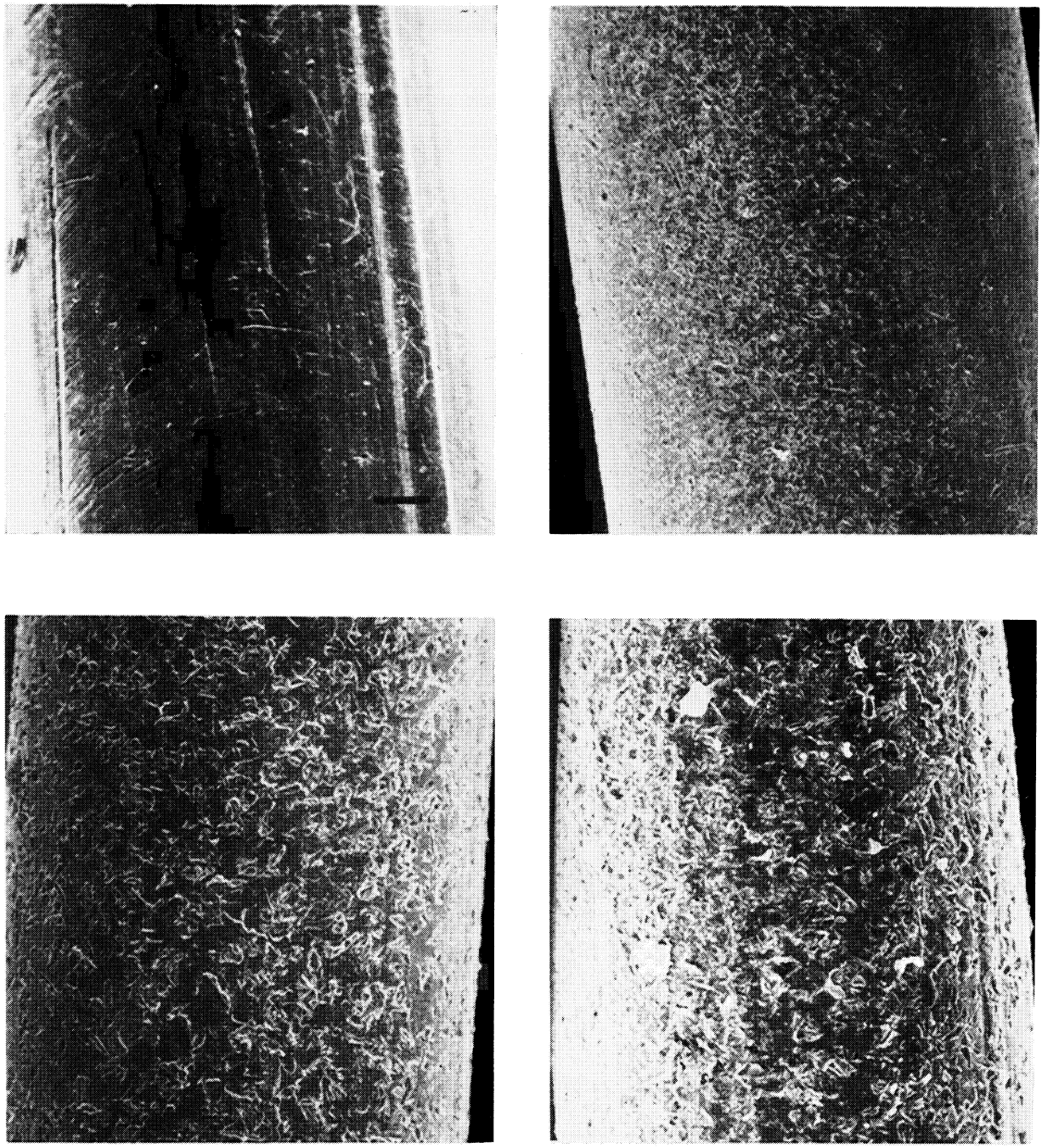

Figure 18. Smooth and roughened stainless steel wires. Scanning electron microscope 200X.

a. Smooth
b. #240 roughened
c. #180 roughened
d. #120 roughened

## NEW TECHNOLOGY APPENDIX

After a diligent review of the work performed under this contract, NAS3-11522, no new technological innovation, discovery, improvement or invention was made.

DISTRIBUTION LIST

| | Number of Copies |
|---|---|
| National Aeronautics and Space Administration<br>Washington, D. C. 20546<br>Attn: Douglas A. Gilstad/RV-2 | 2 |
| NASA-Lewis Research Center<br>21000 Brookpark Road<br>Cleveland, Ohio 44135<br>Attn: D. A. Petrash M.S. 54-1 | 50 |
| Advanced Technology Laboratories<br>General Electric Company<br>Schenectady, New York 12308<br>Attn: R. F. Gaertner | 1 |
| Astronautic/Propulsion<br>Mail Stop 1662<br>Martin Denver Division<br>Denver, Colorado 80201<br>Attn: Howard L. Paynter | 1 |
| Bell Aerosystems<br>Buffalo, New York 14240<br>Attn: Minas Ensanian | 1 |
| Battelle Memorial Institute<br>505 King Avenue<br>Columbus, Ohio 43201<br>Attn: Clarkson L. Coffin<br>Attn: Alan U. Hare | 1<br>1 |
| NASA-Manned Spacecraft Center<br>2101 Webster-Seabrook Road<br>Mail Stop EP-21<br>Houston, Texas 77058<br>Attn: Jerry C. Smithson<br>Attn: Zach D. Kirkland | 1<br>1 |
| Massachusetts Insitute of Tech<br>Cambridge, Massachusetts 02138<br>Attn: Dr. Peter Griffith | 1 |

| | Number of Copies |
|---|---|
| McDonnell-Douglas Corporation<br>3000 Ocean Park Blvd.<br>Santa Monica, California 90406 | |
| Attn: R. A. Madsen | 1 |
| Attn: J. B. Blackmon | 1 |
| Midwest Research Institute<br>435 Volker Blvd.<br>Kansas City, Missouri 64110 | |
| Attn: Dr. Sheldon Levy | 1 |
| NASA-John F. Kennedy Space Center<br>Kennedy Space Center, Florida 32899 | |
| Attn: J. P. Claybourne/MC | 1 |
| Attn: W. H. Boggs/MC | 1 |
| Office National D'Etudes Et De<br>Recherches Aerospatiales<br>29, Avenue de la Division LeClerc<br>92 Chatillon<br>France | |
| Par Michel Delattre | 1 |
| Par Jean Maulard | 1 |
| Southwest Research Institute<br>Department of Mechanical Sciences<br>8500 Culebra Road<br>San Antonio, Texas 78206 | |
| Attn: Dr. H. Norman Abramson | 1 |
| Attn: Dr. Frank Dodge | 1 |
| Space and Information Systems Div.<br>North American Aviation, Inc.<br>12214 Lakewood Blvd.<br>Downey, California 90241 | |
| Attn: Donald J. Simkin | 1 |
| Spacecraft Thermodynamics Dept.<br>Lockheed Missiles & Space Company<br>Sunnyvale, California 94008 | |
| Attn: Dr. H. M. Satterlee | 1 |
| TRW Space Technology Laboratory<br>One Space Park<br>Redondo Beach, California 90277 | |
| Attn: Dr. R. E. Hutton | 1 |
| Attn: Dr. Pravin Bhuta | 1 |

| | Number of Copies |
|---|---|
| General Dynamics - Convair<br>Keonary Mesa Plant<br>Mail Zone 967-93<br>San Diego, California 92112<br>Attn: Mr. George B. Wood | 1 |
| Hughes Aircraft Company<br>Aerospace Group<br>Propulsion Department<br>Space Systems Division<br>El Segundo, California 90045<br>Attn: Lloyd F. Kohrs, Manager | 1 |
| Martin Marietta Corporation<br>Denver Division<br>Propulsion Research Dept.<br>Mail T-1660<br>Denver, Colorado 80201<br>Attn: Dr. T. E. Bowman | 1 |
| NASA-Scientific and Technical Information Facility<br>P. O. Box 5700<br>Bethesda, Maryland 20740<br>Attn: NASA Representative | 3 |